e - ISSN 2586-9396

Current Applied Science and Technology

Vol. 19 No. 1

January - April 2019

KING MONGKUT'S INSTITUTE OF TECHNOLOGY LADKRABANG

Advisory Board

Current Applied Science and Technology or CAST, formerly KMITL Science and Technology Journal, has been established since its inception as KMITL Science Journal in 2001. The journal has been dedicated to publishing advanced and applied knowledge in the form of high quality research and review articles covering the main areas of Biotechnology, Environmental Science, Agricultural Technology, and other fields related to Applied Science and Technology. Special issues devoted to important topics in advanced science and technology will occasionally be published.

The highlight of this journal is to give an opportunity for those researchers with high quality research articles presented at International Conferences such as the International Symposium on Biocontrol and Biotechnology, the International Conference of Biotechnology and Environment, and the International Symposium on Mathematical, Statistical and Computer Sciences organized by various countries, mainly in ASIA, to be published in Current Applied Science and Technology.

The journal is an open access peer-reviewed and double blinded journal using Online Journal System (OJS). Previously, articles were published in print on a regular basis (two issues per year) since 2001 and since 2010 onward the articles have been published both in print and electronic forms starting from volume 10. In 2017, the journal title has been changed from *KMITL Science and Technology Journal* to *Current Applied Science and Technology* (CAST) (e-ISSN 2586-9396) to be more identifiable to the international scientific community according to the suggestion of Thai-Journal Citation Index Centre. The journal has been published online only since volume 2 (July-December, 2017). In addition, the journal has attracted researchers from other countries more than 22% according to the data. The examples of countries where researchers have chosen to publish the articles in CAST are as follows: UK., U.S.A., Australia, Japan, Nigeria, Malaysia, Iraq, Egypt, etc. As of 2017, the number of citation is 203 from 49 countries. Because of more demands on publication in CAST, the editorial board has decided to publish online original academic research and review articles three issues per year (April, August and December) from 2018 onward.

Furthermore, the advisory board and editorial board comprises honorable and wellknown members from around the world in which 50% of editorial board members are from various countries like U.K., Norway, Japan, India, China, Singapore and Egypt. Only 25% of Thai editorial board members are from the publisher organization and 25% from other publisher organizations. Most of advisory and editorial board members have high H-index according to SCOPUS.

The journal is also committed to maintaining the high level of integrity in the content published and has a Conflict of Interest policy in place. The journal uses plagiarism detection software to screen the submissions. The journal has been working closely with Thai-Journal Citation Index Centre to ensure that the journal complies with international standard of SCOPUS.

Current Applied Science and Technology (CAST)

(formerly KMITL Science and Technology Journal)

Editor

Dusanee Thanaboripat
King Mongkut's Institute of Technology Ladkrabang, Thailand

Editorial Board

CONTENTS

Porous Carbon Adsorbent from Humin Derived from Thai Leonardite for Methylene Blue Dye Adsorption

Jutaporn Sayjumpa[1], Buntita Jomhataikool[1], Kajornsak Faungnawakij[2], Sanchai Kuboon[2], Wasawat Kraithong[2], Masayoshi Fuji[3] and Apiluck Eiad-ua[1*]

[1]College of Nanotechnology, King Mongkut's Institute of Technology Ladkrabang , Ladkrabang, Bangkok, Thailand
[2]National Nanotechnology Center, National Science and Technology Development Agency, Pathumthani, Thailand
[3]Advanced Ceramic Research Center, Nagoya Institute of Technology, Tajimi,Gifu, Japan

Received: 15 May 2018, Revised: 27 January 2019, Accepted: 30 January 2019

Abstract

Leonardite is by-product from lignite mine found in northern Thailand. Leonardite is generally known as natural source of humic substances. Humic substances can be divided into three major fractions, i.e. humin, humic acids and fulvic acids. These fractions can be extracted by using solution adjusted to different acid alkaline (pH levels). Humin is a major product that can be extracted from Thai leonardite and it is over 80% yield of product. The morphology of humin is non-conductive bulk material with few porous structures. It can be used as adsorbent for dye adsorption or heavy metal and used as catalyst supporter. The synthesis of porous carbon from humin via carbonization process was investigated in this research. Humin was carbonized at different temperatures and characterized by SEM, FTIR, UV-Vis and BET. Porous carbon from humin was used in methylene blue dye adsorption. The result indicates that the particle size of humin was decreased with well-dispersed and non-agglomerate humin was observed in higher carbonization temperature. The adsorption capacity of humin was increased with increasing of temperature up to 700ºC and decreased at 900ºC according to surface area and porosity results. Although the carbon content of humin was increased at higher temperature, the function group used as adsorbent was decomposed.

Keywords: leonardite, humic substance, humin and carbon absorbent
DOI 10.14456/cast.2019.1

1. Introduction

Dyes dissolved in industrial wastewater are the main problem which cause varied side effects to surrounding environment [1]. Dyes at approx 10-15% was released into water resources exhibiting organic compounds highly resistant to degradation [2]. A large quantity of dyes from various

*Corresponding author: Tel.: 0 2329 8000 ext 3132 Fax: 0 2329 8265
E-mail: apiluck.ei@kmitl.ac.th

industries such as apparel, textile and so on have been used which is the cause of health problems and environmental pollution. Recently, several researchers have reported that the carcinogenic toxicity of dyes is harmful to humans and animals [3]. Hence, promising technologies have been investigated to solve this problem. One of these is adsorption, the process is a well-known method for water decontamination applications because it is simple to design, convenient to use, low-cost for reusability and also, the formation of toxic substances [5]. Various factors related to the adsorption efficiency of dye are based on nature of dyes, pH of adsorbate solution, pH at point zero charge (pzc), porosity and surface functional of adsorbent. There are many types of sorbents that are often studied, such as zeolite, silica and activated carbon [6]. Activated carbon was widely selected for the removal from wastewater since it is a simple process, but the price is still high. Therefore, there is a need for simple and inexpensive materials. From such issues, most researches have focused on natural materials which are easy to find, or may be a by-product or waste material from industries which needs additional cost reduction [7].

Thailand is a significant producer of lignite, which is used almost exclusively for power generation or as source of energy for cement and steam engine industries. Total national lignite production is around 21 million tons per year [8]. In Southeast Asia, Thailand is one of the biggest lignite mines [9] and leonardite is a by-product of lignite mine. In general, leonardite is a rather complex material predominately made of carbon (55% by weight) [10]. Leonardite in nature has about 20-70% organic composition and when passing carbonization process, organic matter can be converted to activated carbon [11]. Leonardite is known as natural source of humic substances. Humic substances have organic complex structures, high molecular weight, and are durable to decay. The decomposition of plant and animal residues results in carbon molecules as components of humic substances. Humic substances are main components of soil, coal, dystrophic lakes and sea water [12]. The properties and detailed structure are based on the condition of soil, water resources and the extraction method [13]. Humic substances can be divided into three major fractions: humin, humic acids and fulvic acids and can be extracted using solution adjusted to different acid alkaline (pH levels). Humin is an organic matter insoluble in water at all pHs forming as dark brown solids which are in homogenous and their structures are often vaguely described. Humic acid and fulvic acid can be extracted from soil and other solid phase using a strong base at high pH. Our previous study found that humin was a major product which was over 80% yield of product whereas humic acid and fulvic acid were only 10-20% of product (unpresented data) and it is possible to improve its properties and used as adsorbent for heavy metal or dye adsorption.

This research was conducted to investigate the feasibility of low-cost adsorbent for methylene blue adsorption. Humin adsorbent was obtained from lignite mines in Lampang province, Thailand. Methylene blue (MB) was chosen as the model dye in this study because of its difficulty to degrade in nature and its strong adsorption onto solids. The effects of temperature in carbonization process and adsorption capacity of humin were studied in this research. The adsorbent capacity was characterized by Scanning Electron Microscope (SEM), Fourier Transform Infrared Spectroscopy (FTIR), Brunauer–Emmett–Teller (BET) surface area and UV-vis spectroscopy, respectively.

2. Materials and Methods

Leonardite was collected from lignite mine at Mae Moh, Lamphang province, Northern Thailand. The sample was dried at 80ºC for 24 h. Afterwards, the soil sample was milled into powder by mortar and sieved for selection of particle size between 180 to 500 μm The extraction of humic substance from leonardite was carried out following the method suggested by Gracia [14], using

base-acid treatment. Soil extraction was performed by mixing 40 g of dry leonardite powder with 400 ml of KOH solutions at concentration of 0.1M solution for 3 h at room temperature. The extracted soluble containing humic acids (HA) + fulvic acids (FA) was further separated from insoluble fraction containing humin by centrifugation at 5000 rpm for 15 min. The humin fraction was dried at 90ºC for 24 h. Dried humin fraction was milled into powder and carbonization at 300, 500, 700 and 900ºC for 2 h. in horizontal furnace under nitrogen (N_2) atmosphere. The humin sample was characterized for morphology, chemical structure, pore volume and BET, surface area by Scanning Electron Microscope (SEM), Fourier Transform Infrared Spectroscope (FT-IR) and Brunauer–Emmett–Teller (BET), respectively. For the adsorption experiment, 1g of humin adsorbents and 25 ppm of methylene blue (25 mg/l) were added to centrifuge tubes. The tubes were centrifuged at 3,000 rpm for 5 min, and the humin adsorbents were filtered through filter paper. The color removal of MB dye solutions was analyzed by measuring the absorbance with a UV-Vis spectroscopy.

3. Results and Discussion

The SEM image in Figure 1 (a, b) of humin (1000x, 2000x magnification) at room temperature indicates that its morphology composed of particles with various shapes and sizes distribution. As a result of the mechanical force, the structure was broken down leading to the agglomeration of small particles in some areas. The humin is non-conductive bulk material with few porous structures and nonuniform. In Figure 1 (c, d, e and f), the morphology and particle size distribution of humin carbonized at different temperatures varying from 300, 500, 700 and 900 ^oC for 2 h in N_2 atmosphere are presented. The result indicates that the particle size of humin was decreased when carbonization temperature was increased. In addition, well-dispersed and non-agglomerate humin particle was observed at higher carbonization temperature because of the evaporation of water and the decomposition of organic matter in humin structure according to FT-IR result.

Figure 2 indicates that solid yield of humin was decreased when carbonization temperature was increased. As a result of thermal degradation, it causes water to evaporate and the organic matter to decompose (as shown in FT-IR result, Figure 3).

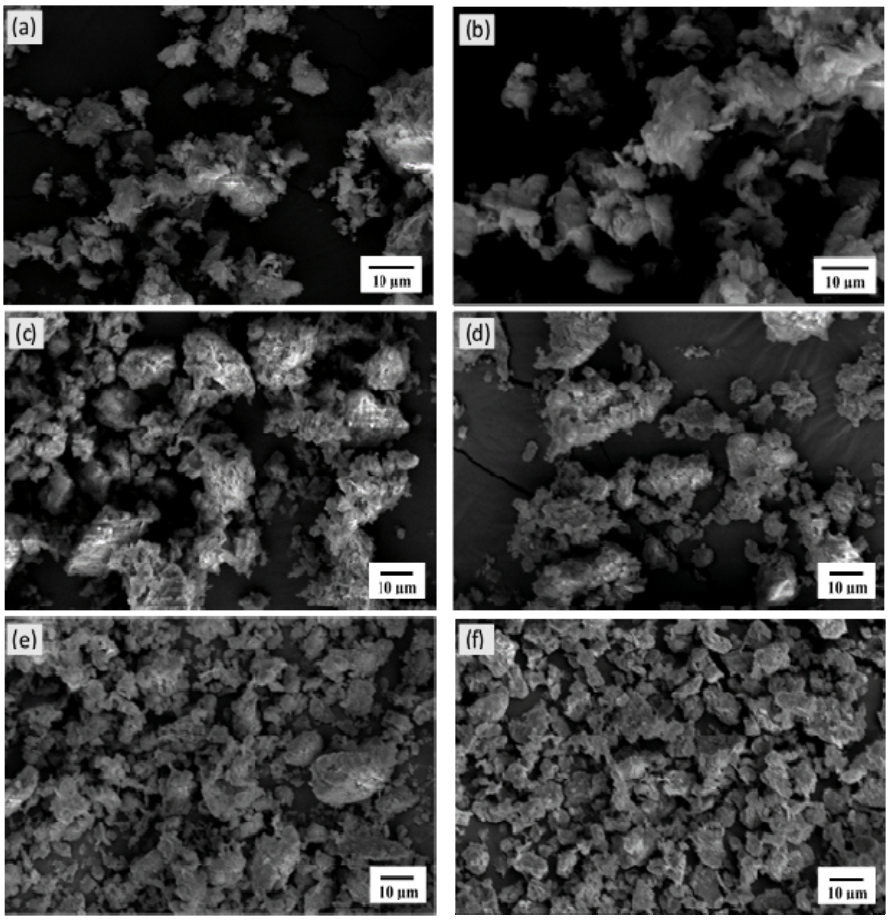

Figure 1. SEM image of (a) Humin at 1000x magnification and (b) at 2000x magnification at room temperature (c) Humin extracted from leonardite soil via carbonization process for 2 h in N_2 atmosphere at 300 ^oC, (d) 500 ^oC , (e) 700 ^oC and (f) 900 ^oC.

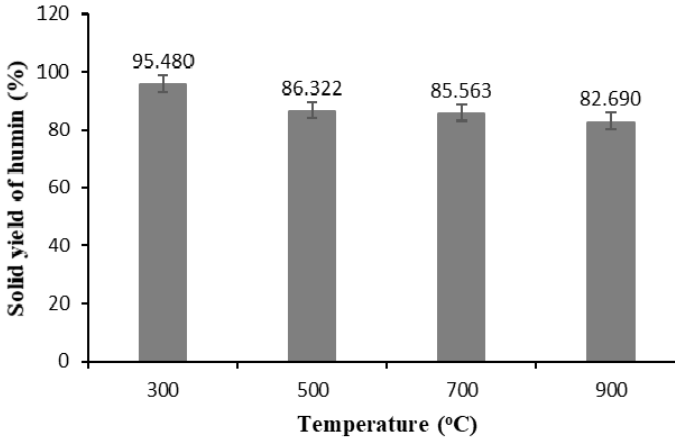

Figure 2. Solid yield of humin extracted from leonardite soil via carbonization process at different temperatures for 2 h in N_2 atmosphere.

The FT-IR spectra of humin via carbonization process at different temperatures for 2 h in N_2 atmosphere recorded in the range of 4000–400 cm^{-1} are presented in Figure 3. The spectra bands were similar in various conditions. The spectra bands were around 3700-3500 cm^{-1}(–OH stretching), 1005 cm^{-1}(C–OH stretch of aliphatic alcohol), 910 cm^{-1}(=C-H stretching) and 700-400 cm^{-1} (aromatic band). The humin at spectra bands around 700-400 cm^{-1}(aromatic band) and carbonized at 300 °C was slightly increased compared to the humin at room temperature. In addition, the spectra bands around 3700-3500 cm^{-1} (O-H stretching) were decomposed at 500 °C due to the evaporation of water. However, the spectra bands around 700-400 cm^{-1}(aromatic band), 1005 cm^{-1}(C–OH stretch of aliphatic alcohol) and 910 cm^{-1}(=C-H stretching) were decreased when carbonization temperature was increased due to the decomposition of organic matter and moisture.

High specific areas and S_{BET} values (1200–1807 m^2/g) were obtained for all AC materials. The results of BET surface area of humin prepared at different temperatures (300, 500,700 and 900 °C) are shown in Table 1, indicated that BET surface areas are quite lower than commercial activated carbons. BET surface area values were higher in cases of increasing carbonization temperature from 300 °C to 700 °C but lower at carbonization temperature of 900 °C. The pore size of humin was almost unchanged and remained at about 3.6-3.9 nm. In addition, pore volume was estimated from nitrogen adsorption at a relative pressure of 0.95 which was similar to that from 300 °C to 700 °C and decreased at 900 °C. This finding can be explained in terms of contraction of some pore wall that blocked and/or reduced the pore size.

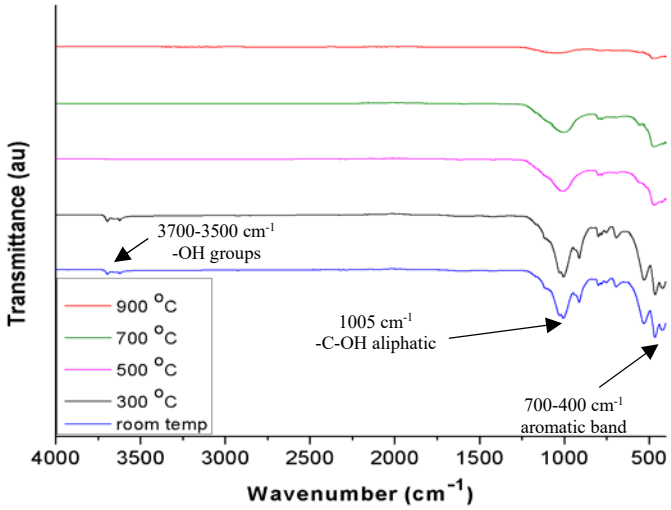

Figure 3. FT-IR spectra of humin via carbonization process with different temperatures for 2 h in N_2 atmosphere.

Table 1. Physical and adsorption properties of humin with different temperatures for 2 h in N_2 atmosphere.

Temperature (°C)	BET surface area (m^2/g)	Pore volume (cm^3/g)	Pore size (nm)
300	29.88	0.10	3.97
500	31.56	0.11	3.69
700	37.45	0.12	3.69
900	16.25	0.07	3.95

Humin carbonization was performed at different temperatures (300, 500,700 and 900 °C) for 2 h. From Figure 4, it can be observed that the adsorption capacity of the methylene blue (MB) on carbonized humin was increased with increasing of carbonization temperature but decreased at 900 °C. Approximately 90% of MB was removed from the solutions with contacting time of 5 min. The result can be explained from BET surface area, pore volume (Table 1) or perhaps there are functional group that are changed with carbonization process which can make MB adsorption capacity of humin better. It might be that the carbonization may increase the adsorption efficiency and it is assumed that increasing of carbonization temperatures can lead to the increase of surface area, pore volume of the adsorbent and the formation of activated carbon. In addition, adsorption capacity is approximately 5 times higher than 80%.

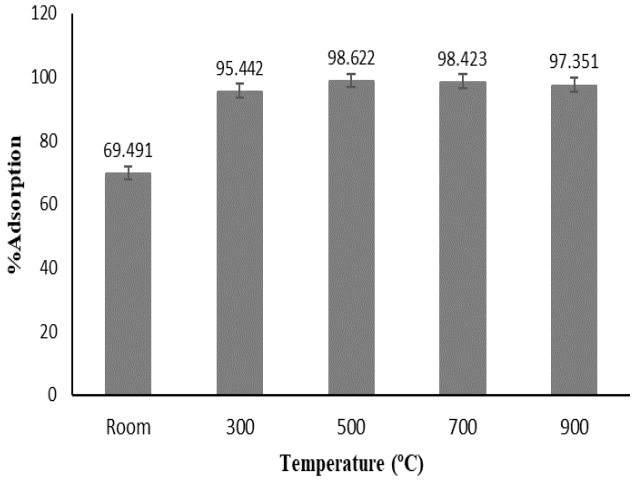

Figure 4. Methylene blue adsorption capacity of humin via carbonization process at different temperatures for 2 h in N_2 atmosphere.

4. Conclusions

The adsorbent has been successfully prepared from humin. Carbonization temperature has a significant effect on particle size, surface area values, pore volume and carbon content leading to adsorption efficiency of humin. Decreasing adsorption capacity may be related to decreasing surface area. The porosity and adsorbent properties could be predicted from this result. It also indicates that these materials used in this work could be effective adsorbents for practical use in the future.

5. Acknowledgements

The authors are grateful to the Research and Researcher for Industry (RRi), The Thailand Reseach Fund (TRF) and Suntitranon Co., Ltd. The authors are also thankful to the National Nanotechnology Center (NANOTEC), National Science and Technology Development Agency (NSTDA) and College of Nanotechnology, KMITL for their support.

References

[1] Metivier-Pignon, H., Faur-Brasquet, C. and Cloirec, P.L., 2003. Adsorption of dyes onto activated carbon cloths: approach of adsorption mechanisms and coupling of ACC with ultra filtration to treat coloured wastewaters. *Journal of Separation and Purification Technology*, 31, 3–11.

[2] Ghodbane, H., Hamdaoui, O., 2009. Intensification of sonochemical decolorization of anthraquinonic dye acid blue 25 using carbon tetrachloride. *Journal of Ultrasonics Sonochemistry*, 16(4), 455-461.

[3] Rafatullah, M., Sulaiman, O., Hashim, R. and Ahmad, A., 2010. Adsorption of methylene blue on low-cost adsorbents: a review. *Journal of Hazardous Materials*, 177, 70–80.
[4] Dabrowski, A., 2001. Adsorption from theory to practice. *Journal of Advances in Colloid and Interface Science*, 93, 135–224.
[5] Gayatri1, S. L. and Ahmaruzzaman, Md., 2010. Adsorption technique for the removal of phenolic compounds from wastewater using low-cost natural adsorbents. *Journal of Science & Technology,* 5(2), 157-166.
[6] Mohammed, M.A., Shitu, A. and Ibrahim, A., 2014. Removal of methylene blue using low cost adsorbent: a review. *Research Journal of Chemical Sciences*, 4, 91-102.
[7] Bailey, S.E., Olin, T.J., Bricka, M. and Adrian, D.D., 1999. A review of potentially low-cost sorbents for heavy metals. *Journal of Water Research*, 33, 2469–2479.
[8] World Energy, 2016. World energy resource 2016, [online] Available at: https://www.worldenergy.org/data/resources
[9] Teparut, C. and Sthiannopkao, S., 2011. Mae Moh Lignite Mine and Environmental Management. *Journal of Geosystem Engineering*, 14(2), 85-94.
[10] Schwarzenbach, R.P., Gschwend, P.M. and Imboden, D.M., 1993. *Environmental Organic Chemistry*. New York : John Wiley & Sons Inc.
[11] Janŏs, P., Michalek, P. and Turek, L., 2007. Sorption of ionic dyes onto untreated low- rank coal oxihumolite: a kinetic study. *Journal of Dyes and Pigments*, 74, 363-370.
[12] Aiken, G.R., McKnight, G.R., Wershaw, R.L. and MacCarthy, P., 1985. *Humic Substances in Soil, Sediment and Water : Geochemistry, Isolation and Characterization.* New York: Wiley.
[13] Berbara, R.L.L. and García, A.C., 2014. Humic substances and plant defense metabolism. In: P. Ahmed and M.D. Wani, eds. *Physiological Mechanisms and Adaptation Strategies in Plants under Changing Environment*. New York : Springer, pp. 297-319.
[14] Garcia, D. and Cegarra, J., 1996. A comparison between alkaline and decomplexing reagents to extract humic acids. *Journal of Fuel Processing Technology*, 48, 51-60.

Influence of Hydrothermal-carbonization Process on Biochar Properties from Cattail Weed Waste

Araya Smuthkochorn[1], Nardnutda Katunyoo[1], Napat Kaewtrakulchai[1], Duangduen Atong[2], Kanit Soongprasit[2], Masayoshi Fuji[3] and Apiluck Eiad-ua[1*]

[1]College of Nanotechnology, King Mongkut's Institute of Technology Ladkrabang, Bangkok, Thailand
[2]National Metal and Materials Technology Center (MTEC), Bangkok, Thailand
[3]Advanced Ceramic Research Center, Nagoya Institute of Technology, Tajimi, Japan

Received: 9 May 2018, Revised: 20 November 2018, Accepted: 29 January 2019

Abstract

Biochars have been successfully synthesized from Cattail leave (CL) via hydrothermal and carbonization process. The experimental work described has focused on physical properties of biochars produced from Cattail leaves at 160, 180 and 200°C for 8, 12 and 24 h for hydrothermal and substituted to carbonization at 700°C for 2 h. The influences of hydrothermal and carbonization on the pore structure, surface functional groups and the product yield was also investigated by characterization using Scanning Electron Microscope (SEM) and Fourier Transform Infrared Spectroscopy, respectively. Although the morphologies of cell structures were maintained in the hydrothermal and carbonization, it was found that the yield of produced biochar was decreased with increase of the hydrothermal temperature and time. The images from SEM showed that the pore structures are quite roughness on their external surface of biochar and the functional group of their surface area has most of pure carbon content (59-65 wt%).

Keywords: Cattail leaves, Carbonization, Hydrothermal, Biochar
DOI 10.14456/cast.2019.2

1. Introduction

A wide range types of biomass have been utilized for energy, conversion options, end-use applications and infrastructure requirements [1]. Biomass is derived from agriculture waste such as coconut shell, palm shell, rice straw, coffee ground, etc. [2-3], harvesting forestry and other plant residues. The biomass feedstocks have been collected, transported and possibly stored, before being processed into a suitable form for energy conversion technology [4-5]. The energy produced from used of biomass is only one of renewable energy that can reduce the impact of energy production, in which there are many ways to minimize such effects as a GHG emissions.

*Corresponding author: Tel.: +66 (0)2329 8000 Ext. 3132 Fax: +66 (0) 2329 8265
E-mail: apiluck.ei@kmitl.ac.th

Cattail wetland plants are weed found in all area throughout Thailand, generally grow and spread vigorously under the right conditions through their root systems and seed. The seeds germinate rapidly under hot, moist conditions and can be ready for transplant in just a few months, which gives the main cause of the flooding and spoiling. Cattail leaves can be used as the cheapest source for energy production, carbon sequestration, and as an essential element for the production of hydrochars and active carbons [6]. In the past few years, the conversion of biomass waste into valuable carbon materials has received considerable attention due to the ability to produce hydrochars with attractive characteristics that promote efficiency for a variety of applications [7-12] such as supporting materials for environment, energy technology and improvement of bio-oil properties [13].

Traditionally, carbonization is a thermochemical conversion process that can be applied for the development of biomass to carbon materials. On the other hand, hydrothermal-carbonization is the technique to modify chemical structure using water for conversion of biomass to carbon products which gives higher yield than carbonization [14-17]. Most organic matters in raw materials for feedstocks are transformed into solid, depending on the temperature and time via hydrothermal-carbonization process. The formation of biochar from lignin materials via direct solid conversion of biomass formation [18] and polymerization or condensation monomer generated from decomposition of biomass are proposed [19].

In this study biochar was prepared from Cattail leaves by hydrothermal and carbonization process. The produced biochars were characterized by Scanning Electron Microscope, Elemental Analyzer and Fourier Transform Infrared Spectroscopy. This research work aims to study the effects of hydrothermal-carbonization temperatures and times on the pore structure, elemental contents, surface functional groups and yields of resulting product. The potential applications of biochar derived cattail leaves as an alternative energy were also examined.

2. Materials and Methods

2.1 Preparation of raw material

Lignocellulosic biomass from Cattail leaves (CL)(*Typha angustifolia* Linn.) was used as raw material for producing biochar. Cattail is generally a weed that can be found in all areas throughout Thailand. Cattail leaves biomass were dried at 110°C for 24 h to remove moisture, then crushing into smaller size using a knife mill.

2.2 Hydrothermal-carbonization of Cattail leaves

Regarding biochar production, 20 grams of CL biomass were mixed with 400 ml of deionization water and then reformulated with hydrothermal at 160, 180 and 200°C for 8, 12 and 24 h in stainless-steel chamber. Then, the samples were carbonized at 700°C under nitrogen flow in stainless-steel reactor for 1 h by a ramp rate at 10°C/min. All experimental conditions for biochar derived from CL were shown in Table 1. The resulting biochar produced at 160, 180 and 200°C for 8, 12 and 24 h was labeled as CL-160-8, CL-160-12, CL-160-24, CL-180-8, CL-180-12, CL-180-24, CL-200-8, CL-200-12 and CL-200-24, respectively.

Table 1. Conditions of biochar derived from Cattail leaves.

Sample	Temperature (°C)	Time (h.)
CL-160-8	160	8
CL-160-12	160	12
CL-160-24	160	24
CL-180-8	180	8
CL-180-12	180	12
CL-180-24	180	24
CL-200-8	200	8
CL-200-12	200	12
CL-200-24	200	24

2.3 Characterization of biochar derived from Cattail leaves

The production yield of biochar was calculated with applied formula as follows:

$$Y\ (\%) = m/m_0 \times 100$$

Where Y is the yield (%) of produced biochar, m is mass of produced biochar (g), and m_0 is raw cattail leaves biomass (g).

In order to observe the pore structure, elemental contents and surface morphologies of CL derived biochar with different hydrothermal-carbonization conditions, these samples were examined using high-resolution scanning electron microscopy (SEM, Zeiss EVO MA 10). Due to the chemical compositions of biochar products rich in lignocellulosic components, the elemental analysis of resulting materials was conducted using an elemental analyzer (Elementar, Vario EL III) in terms of carbon (C), hydrogen (H) and nitrogen (N) wt%. The surface functional groups of biochar were analyzed by Fourier-Transform Infrared Spectroscopy (FT-IR, Perkin Elmer Spectrum). The spectra were performed between 4000-400 cm^{-1} to observe the influences of hydrothermal-carbonization conditions on the efficiency of carbon conversion to the biochar products.

3. Results and Discussion

3.1 Yield of biochar products

The thermal decomposition of biochar during hydrothermal-carbonization experiment produced three products including solid char, condensable liquid and non-condensable gas, the relative amounts of three products depend on experimental conditions. The yield of biochar is defined as the ratio of the weight of biochar after carbonization to the weight of the raw materials as seen from the applied formula in previously reported [20]. On the other hand, the hydrothermal temperature and time play an important role in the yield (%) of biochar. As seen from Figure 1 the yield of resulting biochar products decreased, this is due to the loss of volatile materials with increasing hydrothermal-carbonization temperature and time. It should be noted that the yield (%) of the resulting biochar prepared at a specific hydrothermal temperature for the hydrothermal time of 24 h (CL-160-24, CL-180-24 and CL-200-24 was about 43.04, 41.77 and 47.29% respectively)

was higher than the hydrothermal time (8 and 12 h), the presence of time promotes the re-polymerization [21] of constituent biopolymer, hydrothermal sample is influenced by hydrolysis which is the determining first step that exhibits water soluble organic compounds. The solid product is subsequently formed by re-condensation reaction of soluble organic compounds in water, resulting in the increased yield of biochar. The availability of the fragments from hydrolysis in the liquid phase offers a huge potential to influence product characteristics due to the excessive duration of holding time during hydrothermal carbonization.

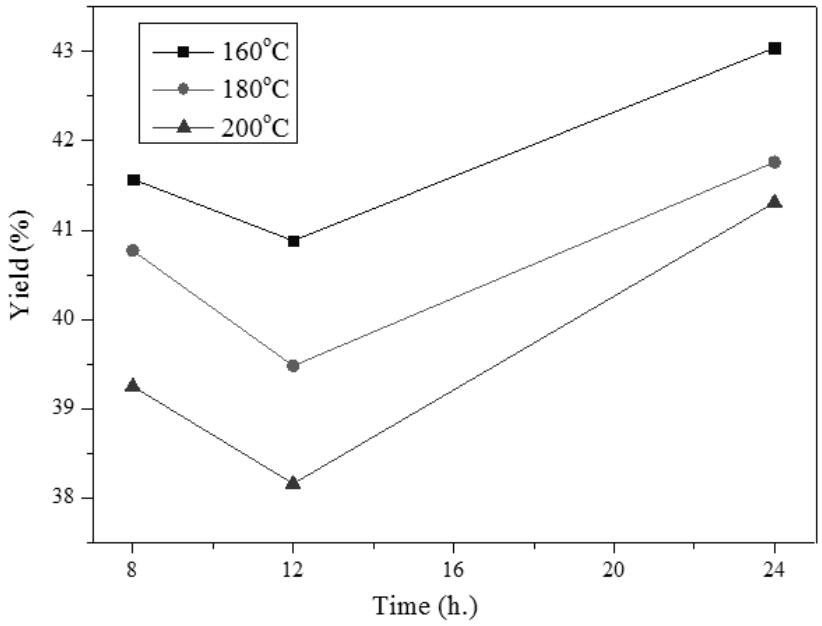

Figure 1. The effect of hydrothermal-carbonization temperature and time on the yield of biochar products.

3.2 Morphology of the resulting biochar products under SEM observation

Scanning Electron Microscope (SEM) measurements were performed using SEM Zeiss EVO MA10 operated at 10 kV to observe the surface morphology and pore structure of resulting biochar products derived from Cattail leaves biomass. Figure 2 (a-i) shows SEM image of biochar hydrothermal-carbonization at 160, 180 and 200°C for 8, 12 and 24 h, respectively. The biochar sample displayed a much rougher and irregular surface textures when the temperature and time of the hydrothermal-carbonization increased. However, at the highest hydrothermal time (24 h), the pore structure was changed due to heat shrinkage as shown in Figure 2 (c), (f), (i). A various cavity on their surface resulted from the thermal decomposition of lignocellulosic polymer (i.e. cellulose, hemicellulose and lignin). Under the experimental conditions, a hydrothermal temperature of 200°C for 12 h as seen in Figure 2 (f) was found to be the optimization of pore structure for desired biochar product.

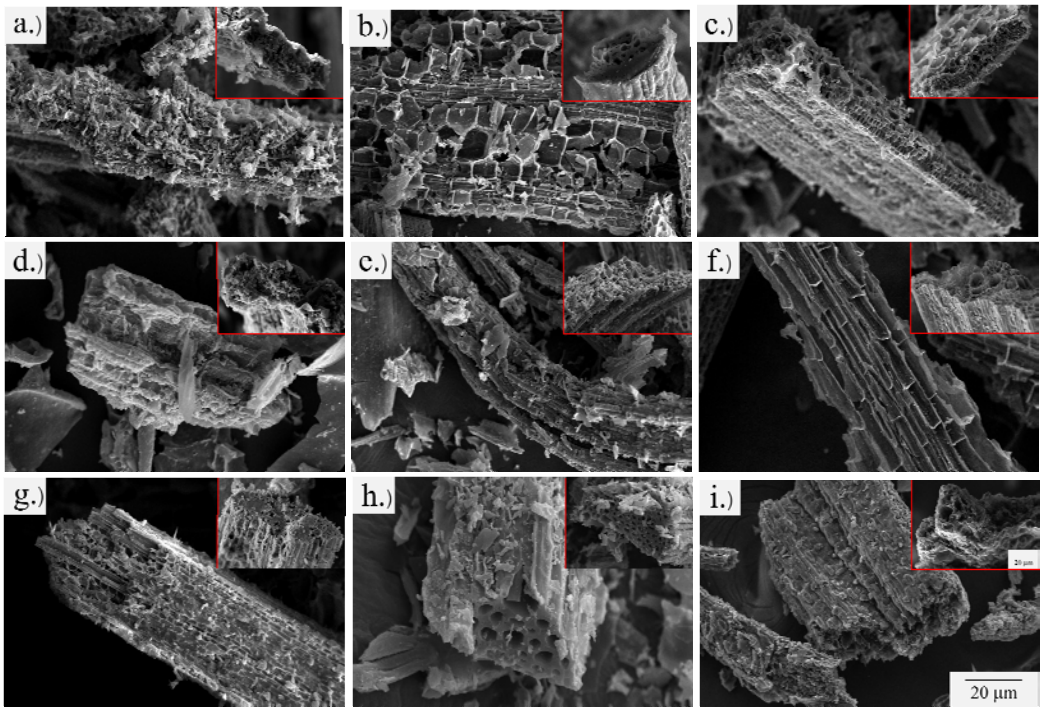

Figure 2. SEM images (300X, 500X) of biochar products from hydrothermal-carbonization at (a) 160°C-8 h. (b) 160°C-12 h. (c) 160°C-24 h. (d) 180°C-8 h. (e) 180°C-12 h. (f) 180°C-24 h. (g) 200°C-8 h. (h) 200°C-12 h. (i) 200°C-24 h.

3.3 Elemental analyses of biochar products

The results of CHN contents are shown in Table 2. The analysis was done by using elemental composition of HTC products. Obviously, theses products were rich in carbon contents, which should be derived from lignocellulosic materials as Cattail leaves biomass. The carbon contents in the biochars were around 59-65 wt%, thus resulting in relatively high carbon contents. It should be noted that the hydrogen contents of resulting biochars at specific hydrothermal-carbonization temperature for the hydrothermal time at 24 h were higher than at 12 and 8 h, which could be attributable to the efficiencies of carbon at the long hydrothermal holding time. In contrast, the carbonization process could create more percentage of carbon content. In comparison, the elemental contents of a typical carbon product used in alternative application such as carbon sorbent (activated carbons) was found to be more percentage of carbon content (above 70%). More interestingly, an increase in the textural pore characteristic of biochar products is associated with increasing hydrothermal-carbonization temperature and holding time. Carbon content (%) was also increased while hydrogen and nitrogen contents were decreased.

Table 2. Elemental contents of biochar products

Sample	C (wt%)	H (wt%)	N (wt%)
CL-160-8	61.720	0.762	1.390
CL-160-12	63.931	0.175	1.501
CL-160-24	60.613	0.705	1.408
CL-180-8	61.406	0.792	1.635
CL-180-12	61.566	0.730	1.433
CL-180-24	64.411	0.127	1.829
CL-200-8	59.521	0.474	1.867
CL-200-12	60.516	0.685	1.794
CL-200-24	60.987	0.724	1.844

3.4 Functional group of biochar products

The carbon matrix does not consist of carbon atoms alone, but is bonded with any atoms like oxygen, hydrogen and nitrogen, etc. These govern the surface chemistry of the biochar products [22]. Infrared spectroscopy provides the functional group on the surface area of products and depending on the precursor and the synthesis steps. The bands of biochar observed in Figure 3 after hydrothermal-carbonization were characterized by using Fourier-Transform Infrared Spectroscopy (FT-IR, Perkin Elmer Spectrum). Considering the FTIR spectra of the biochars as described by Lu *et al.* [23] with the bands covering similar or the same wavelength as observed for the investigated carbon, the FTIR spectra of biochar derived from Cattail leaves also show strong bands at 1000-930 cm^{-1} due to the C-O and C=C stretching vibrations which was related to cellulose and hemicellulose usually found in any plants. The bands at 1600 cm^{-1} are due to vibration mode of C-O stretching and are designated as the lignin group. The bands at 2920 cm^{-1}, C-H stretching are also designated as the lignin group. The region from 3420-2840 cm^{-1} represents the O-H stretching vibrations and is designated as the surface functional group in hydroxyl group and water. Moreover, the bonding of carbon to the other atoms contained in the raw materials such as nitrogen, oxygen and hydrogen is found. These are the bonds of organic compounds in the biomass and after hydrothermal carbonization the bonding of these compounds is destroyed due to the hydrolysis from water and thermal cracking from thermal treatment, resulting in the peaks of the FTIR spectrum. The intensity of the compounds such as C-N is extremely low and cannot be observed in the FTIR results.

FTIR spectra of biochar products with different hydrothermal temperatures and times are illustrated in Figure 3 and percentages of surface functional group that appeared on the surface of resulting materials (calculated by integrated information obtained from the graph) are represented in Figure 4. By considering the percentage of functional group with an increasing hydrothermal temperature, a number of change was found in the bands approximately at 1000-930, 1600 and 2920 cm^{-1} with the presence of carbon vibrations around 2-30%. It could be explained that there was the transformation of organic compounds to carbons. The relative intensity of the bands at approximately 3420-2840 cm^{-1} decreases about 10% when compared to their intensity of Cattail leaves precursor, which is resulted from the evaporation of water molecules during the process. However, it can be noticed that all carbons are observed at the bands of 1600 and 2920 (Figure 3). The bands between around 1000-930 cm^{-1} have often been observed for carbons and carbonaceous materials [24]. The increased temperature and carbonization holding time also exhibits more releasing of volatile substances and represented as high purity of carbon product.

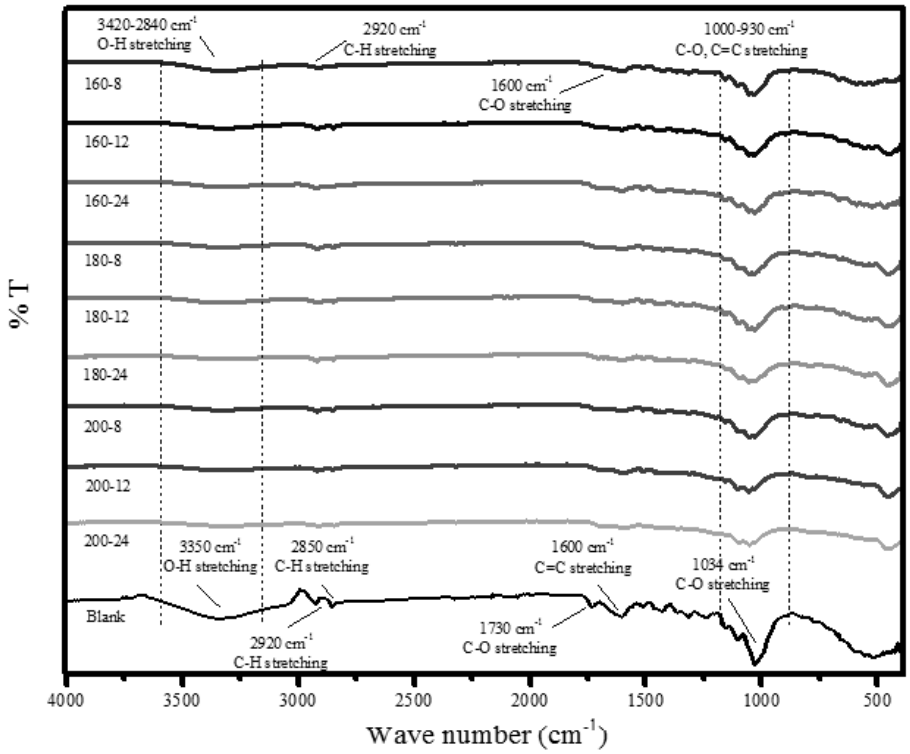

Figure 3. FTIR spectra of the biochar products prepared by hydrothermal-carbonization at different temperatures and times.

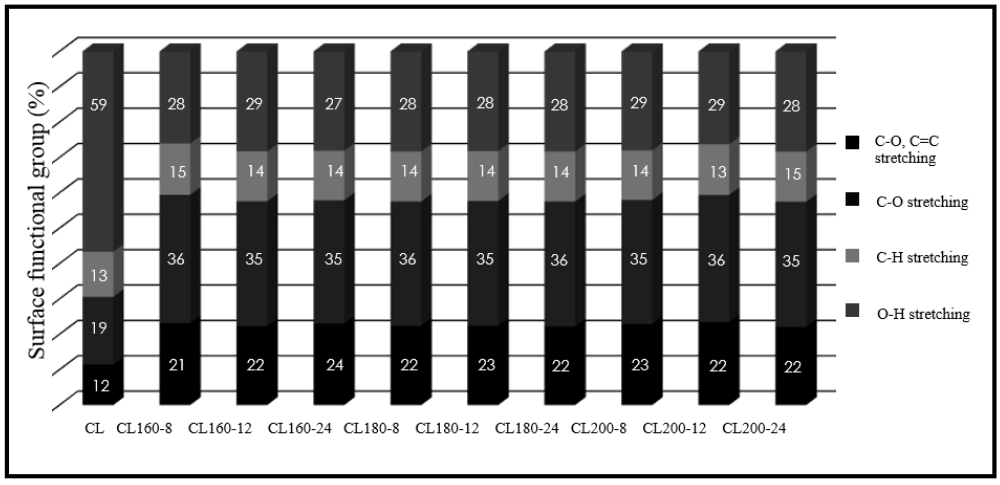

Figure 4. Percentages of the surface functional group of the biochar products prepared by hydrothermal-carbonization at different temperatures and times.

4. Conclusions

This study represents high potential of biochars prepared from Cattail leaves biomass via hydrothermal-carbonization process. Hydrothermal temperature significantly affects the pore development, elemental contents and surface functional group of biochars. The yields of resulting products produced by hydrothermal-carbonization process are higher than only carbonization process. The pore properties of resulting materials and carbon conversion efficiencies are increased. More interestingly, the resulting biochars have significant carbon contents of 59-65 wt%, with lower nitrogen and hydrogen contents. Further study should be investigated on conversion of biomass to be used as alternative energy.

5. Acknowledgements

The authors would like to thank the College of Nanotechnology, King Mongkut's Institute of Technology Ladkrabang (KMITL), Bangkok, Thailand and the financial support of the National Metal and Materials Technology Center (MTEC) via the YSTP program of National Science and Technology Development Agency (NSTDA), Pathumthani, Thailand (Grant GNA-CO-2560-4662-TH/2560) for their supports.

References

[1] Devid, P., Scoot, H., 1986. *Market Assessment of Biomass Gasification and Combustion Technology for Small- and Medium-Scale Applications*: A national laboratory of the U.S. Department of Energy.

[2] Satya Sai, P.M., Ahmed, J., 1997. Production of activated carbon from coconut shell char in a fluidized bed reactor. *Industrial and Engineering Chemistry Research*, 36 (9), 3625-3630.

[3] Donni, A., Wan, M., Mohd, K., 2005. Prepration and characterization of activated carbon from palm shell by chemical activation with K_2CO_3. *Bioresorce Technology*, 98, 145-149.

[4] Peter, M., 2001. Energy production from bimass (part 2) conversion technology. *Bioresorce Technology*, 83, 47-54.

[5] Kacem, M., Pellerano, M., 2015. Pressure swing adsorption for CO_2/N_2 and CO_2/CH_4 separation: comparison between activated carbons and zeolites performances. *Fuel Process Technology*, 138, 271-283.

[6] Liu, Z., Zhang, F.S., 2009. Removal of lead from water using biochars prepared from hydrothermal liquefaction of biomass. *Journal of Hazardous Materials*, 167, 933-939.

[7] Liu, Z., Zhang, F.S., 2010. Characterization and application of chars produced from pinewood pyrolysis and hydrothermal treatment. *Fuel*, 89, 510-514.

[8] Selvi, B.R., Jagadeesan, D., Suma, B., Nagashaniar, G., Arif, M., Balasubramanyam, K., Eswaramoorthy, M., Khudu, T.K., 2003. Intrinstically fluorescent carbon nanosphere as a nuclear targeting vector: delivery of membrane-impermeble molecule to modulate gene expression in vivo. *Nano Letters*, 8(10), 3182-3188.

[9] Titirici, M., Antonietti, M., Thomas, A., 2006. A generalized synthesis of metal oxide hollow spheres using hydrothermal approach. *Chemistry of Materials*, 18(16), 3808-3812.

[10] Sevilla, M., Fuertes, A., Mokaya,R., 2011.High density hydrogen storage in superactivated carbons from hydrothermally carbonizrd renewable organic materials. *Energy and Enviromental Science*, 4, 1400-1410.

[11] Sevilla, M., Fuertes, A.B., 2011. A superior performance for carbon dioxide capture. *Energy and Enviromental Science*, 4, 1765-1771.
[12] Faisal, A., Sahu, J.N., 2011. Optimization and characterization studies on bio-oil production from palm shell by pyrolysis using response surface methodology. *Biomass and Bioenergy*, 35, 3604-3616.
[13] Chao, C., Wha-Seung, A., 2011. CO_2 capture using mesoporous alumina prepared by a sol–gel process. *Chemical Engineering Journal*, 166, 646-651.
[14] Sevilla, M., Macia-Agllo, J.A., Fuerest, A.B., 2011. Hydrothermal carbonization of biomass as a route for the sequestration of carbon dioxide chemical and structural properties of the carbonizaed products. *Biomass and Bioenergy*, 33, 3152-3159.
[15] Kamimura, Y., Shimomura, M., Endo, A., 2016. CO_2 adsorption–desorption properties of zeolite beta prepared from OSDA-free synthesis. *Microporous and Mesoporous Materials*, 219, 125-133.
[16] Jarosław, S., Urszula, N., Antoni, W.M., Rafał, J.W., Beata, M., 2017. Highly microporous activated carbons from biomass for CO_2 capture and effective micropores at different conditions. *Journal of CO_2 Utilization*, 18, 73–79.
[17] Berge, N.D., Ro, K.S., Mao, J., Flora, J.R.V., Chappell M.A., Bae, S., 2011. Hydrothermal carbonization of municipal waste streams. *Environmental. Science and Technology*, 45(13), 5696-5703.
[18] Minkova, V., Razvigorova, M., Goranova, M., Ljutzkanow, L., Angelona, G., 1991. Effect of water vapor on the pyrolysis of solid fuel. *Fuel,* 71, 263-265.
[19] Gergova, K., Galushko, A., Petrov, N., Minkova, V., 1992. Investrigation of the porous structure of activated carbons prepared by pyrolysis of agricultural by-products in a stream of water vapour.. *Biomass and Bioenergy*, 30, 721-730.
[20] Dilek, A., 2013. Effect of pyrolysis temperature and heating rate on biochar obtained from pyrolysis of safflower seed press cake. *Bioresource Technology*, 128, 593-597.
[21] Ayillath, K., Paresh, L., 2015. Lignin depolymerization into aromatic monomer over solid acid catalysts. *ACS Catalysis*, 5(1), 365-379.
[22] Solum, M.S., Pugmire, R.J., Jagtoyen, M., Derbyshire, F., 1995. Evolution of carbon structure in chemically activated wood. *Carbon,* 33, 1247-1254.
[23] Lu, C., Bai, H., Wu, B., Su, F., Hwang, J.F., 2008. Adsorption of Carbon Dioxide from Gas Streams via Mesoporous Spherical-Silica Particles. *Energy and Fuels*, 489-496.
[24] Serafin, J., Narkiewicz, U., Morawski, A.W., Wróbel, R.J., Michalkiewicz, B., 2017. Standing out the key role of ultramicroporosity to tailor biomass-derived carbons for CO_2 capture. *Journal of CO_2 Utilization*, 230, 73-79.

Effect of Thickness of Spring Wire on the Strength and Deformation Characteristics of a Spring Steel Conduit

Kris Sangthong, Wimonwan Ponuam and Rachsak Sakdanuphab*

College of Advanced Manufacturing Innovation, King Mongkut's Institute of Technology Ladkrabang, Bangkok, Thailand

Received: 10 September 2018, Revised: 18 January 2019, Accepted: 12 February 2019

Abstract

In automotive industry, spring steel conduit is a main part of control cables in parking brake, tailgate and transmission. The structure of spring steel conduit consists of liner, steel wire and coating. The steel wire plays an important role in supporting cable exert the force. However, steel wire thickness is concerned with the mechanical strength, flexibility and production cost. In this work, the effects of steel wire thickness on mechanical and physical characteristics of spring steel conduit were investigated. The thickness of steel wire was varied from 0.3 to 0.6 mm. The analysis was performed by JASO T001-97 standard and Hooke's law was used to describe the spring steel conduit. The experimental result was confirmed by the compression testing and agreed with theoretical calculation. It was found that there was an increase in yield stress and young's modulus when the steel wire thickness increased. The compression force at yield that affects deformation in the spring steel conduit was also found. The deformation and stiffness were increased while the steel wire thickness increased. In addition, the minimization of steel wire thickness of 0.4 mm was obtained under JASO T001-97 standard, including the compression force at least 1,000 N and the safety factor of 1.5.

Keywords: Compression force, JASO T001-97 standard, tensile testing, spring steel conduit
DOI 10.14456/cast.2019.3

1. Introduction

Thailand ranks the 12th largest automobile manufacturer in the world and Thailand is ASEAN's leader in the auto parts industry in 2017. The automobile and auto parts export value reach 19,844.69 million dollar with a 15.5% increase from 2016. The control cable manufacturing is one of the auto parts industries. It has an important role to control the mechanical systems of automobiles and motorcycles with a functional safety. The control cable such as parking brake [1-2], tailgate, hood release, fuel lid, door lock, transmission and seat cable are also composed of a spring steel conduit [3]. Due to the various applications, spring steel conduit was following a specification test standard such as ASTM, JASO and JIS. It can ensure vital features of spring steel conduit in consistent. In general, the material properties such as stiffness, light weight, toughness and resistance to tensile loading are concerned in the parts of spring steel conduit [4].

*corresponding author: E-mail: rachsak.sa@kmitl.ac.th

The strength and stiffness of component materials are usually of primary concern. It can be measured in terms of either the stress necessary to cause appreciable plastic deformation or the maximum stress that the material can withstand. Typically, high-strength steels have limited formability, bending and flexibility that decrease even more as strength increases. Thus, the size of material is becoming a critical condition [5-6]. For control cable, it is not only considered on the size of conduit, but also max stress must be considered due to the different functions of each control cable. For example, parking brake control cable has a higher max stress on their structure than the transmission control cable with a high operation forces on lever side. Therefore, the size of transmission control cable [7] is rather thicker than parking brake control cable around 2 mm for the same vehicle types.

In this study, we focus on the effects of steel wire thickness on strength and deformation characteristics of a spring steel conduit. Currently, the 0.6 mm of steel wire has also been used on the clutch control cable and throttle control cable. To provide the advantages of cost reduction, the steel wire thickness of 0.3 mm, 0.4 mm, 0.5 mm and 0.6 mm should be considered. Our experimental results were validated using the calculation based on Hooke's law. The analysis was performed by tensile testing machine under JASO T001-97 standard [8]. The standard determines the compression force must be at least 1,000 N and the safety factor of 1.5 is always taken. The experimental and theoretical analyses has been mentioned for mechanical and physical characteristics of spring steel conduit.

2. Materials and Methods

2.1 Spring steel conduit structure

The spring steel conduit has a standard design according to the JASO T 001-97 standard. The typical structure composes of liner, steel wire and coating as shown in Figure 1. The innermost of spring steel conduit is a liner which has an important role to reduce friction between inner wire and spring steel in the transmission of the push-pull force. A high strength steel wire is converted to a spring core, which is the main structure of spring steel conduit. It represents a flexible composite structure [9-11] with the axial spiral anisotropy of properties, formed by a lay of steel wire. Furthermore, it is suitable for installation onto a curved area. The coating is the outermost layer for protecting the main structure, including spring steel and liner from water, moisture and dust.

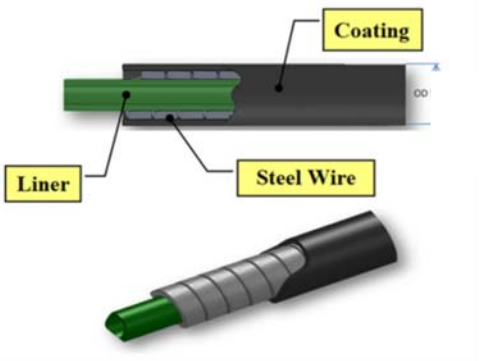

Figure 1. Structure of spring steel conduit consisting of liner, steel wire and coating.

In the production, the spring steel conduit samples were made by the following 3 processes. Rolling is the process of reducing the thickness or changing the cross section of the steel wire. It is a critical process to make spring core using the different steel wire sizes. In the winding process, the steel wire was conducted into a squeeze roll throughout the die before rolling or wrapping around the liner feeder. The last process is a coating. Plastic is used to coat a spring steel conduit through the die injection with OD control around 5 mm. In general, plastic is usually used to coat the spring steel such as PP, PVC, PE and TPEE, etc. that depends on the application.

2.2 Theoretical analysis of spring steel conduits

Spring steel conduits or samples with different steel wire thickness were produced in the production process. The mechanical properties can be described by stress-strain curves [12-15]. The stress-strain relationship can be explained in Figure 2 (a). The stress-strain curves [16] with six different regions are consisted of proportional limit (OA), elastic limit (A), yield stress point or upper yield stress point (B), lower yield stress point (C), ultimate stress point (D) and breaking or rupture point (E). In elastic deformation, the stress-strain relationship is based on the Hooke's law (OA region). It can calculate the young's modulus of the samples to explain strength and stiffness. Figure 2 (b) shows the stress-strain curve with different material such as carbon steel and rubber. It can be clearly seen that the curves exhibit a different characteristic. Carbon steel has a tensile strength stronger than rubber. Carbon steel [17] is a strong material which is not ductile. It has a low stretch and break suddenly. It has a lot of elastic strain energy in a steel wire under tension. Rubber has a large strain for a small stress and it has a small elastic region.

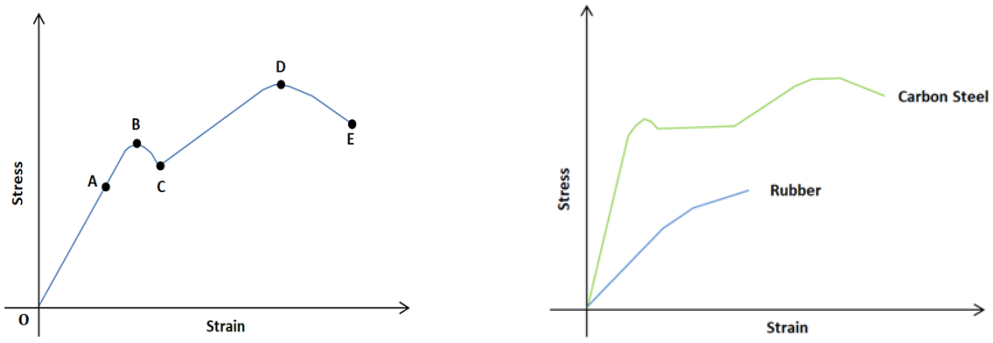

(a) (b)

Figure 2. Stress-strain curves (a) stress-strain curve with different regions and points; (b) stress-strain curve with different material.

The tensile test under JASO T 001-97 standards was employed on the samples for the mechanical response. It can predict the load that affects fracture or deformation in the samples. The analysis is based on stress-strain curve. The sample is experiencing a stress defined to be the ratio of the force (F) to the cross sectional area (A) of the spring steel conduit [1], following by

$$\sigma = \frac{F}{A} \tag{1}$$

Strain is the ratio between the deformation or the changes length (ΔL) with the original length (L_0) [18]

$$\varepsilon = \frac{\Delta L}{L_0} \tag{2}$$

In the low strain portion of the curves, most of materials obey Hooke's law. The stress is proportional to strain with the constant of proportionality being the young's modulus (*E*) [18,19]. Hooke's law along the z-direction, following by

$$E = \frac{\sigma_z}{\varepsilon_z} \tag{3}$$

Where E is Young's modulus, σ_z is the stress along the z-direction and ε_z is strain along the z-direction.

2.3 Material characterization

In general, the spring steel conduit was composed of several materials depend on the application. Polyethylene resin (PE)[20] is a general liner with a high-quality and low-density. The heat resistance is in the range of -40 to 80℃. The properties of PE resin are described in Table 1. High carbon steel wire or SWRH62A is also known as a black wire. It is a drawn steel wire which contains approximately 0.59% to 0.66% of carbon. The chemical compositions of each element are specified in Table 2, following by JIS G 3506: 2004 standards. Polypropylene (PP) [21] resin is used to coat the spring steel wire. The heat resistance is in the range of -40 to 140℃. The density of PP is between 0.895 and 0.92 g/cm³. Therefore, PP is the commodity plastic with the lowest density. The properties of PP resin that we used in this study were referenced by ASTM standard as shown in Table 3.

Our experiment was validated by theoritical calculation based on Hooke's law to confirm the validity of tensile testing. The thickness of steel wire was varied from 0.3 mm to 0.6 mm. The stress, strain, young's modulus, yield stress, compression force, deformation and stiffness were presented and discussed. In addition, the JASO T 001-97 standard was taken into account.

Table 1. The properties of PE resin used in this study were referenced by ASTM standard.

Item	Specification	Unit	Method
Density	0.09 ± 0.02	g/cm³	ASTM D 1505
Tensile Strength	≥ 14	MPa	ASTM D 638
Elongation at Break	≥ 320	%	ASTM D 638
Shore Hardness D Scale	55~69	D scale	ASTM D 2240

Table 2. The properties of high carbon steel wire used in this study were referenced by JIS G 3506: 2004 standard.

Symbol of Grade	Fe	C	Si	Mn	P	S
SWRH62A	97.79	0.59~0.66	0.15~0.35	0.30~0.60	0.30 max	0.30 max

Table 3. The properties of PP resin used in this study were referenced by ASTM standard.

Item	Specification	Unit	Method
Density	0.09 ± 0.02	–	ASTM D 1505
Ash Constant	–	%	Firing
Tensile Stress at Yield	≥ 14	MPa	ASTM D 638
Elongation at Break	≥ 320	%	ASTM D 638
Durometer Hardness D Scale	55~69	D scale	ASTM D 2240
Flexural Modulus	390~690	MPa	ASTM D 790

3. Results and Discussion

The experimental results were carried out by compression testing machine to evaluate mechanical characteristic of spring steel conduit. The stress-strain curves of the samples with different thicknesses of steel wire are presented in Figure 3(a). The results show that the thickness of steel wire directly affected their mechanical behavior such as elastic deformation, first defect and plastic deformation. The first defect is defined as a point which is linearity loss and start of damage in the spring steel conduits. Figure 3(b) shows the example of the first defect on 0.5 mm steel wire thickness. It is occurring at 3.73% strain. It causes by the distortion, but the sample is still usable. The plastic deformation of 0.5 mm steel wire thickness is shown in Figure 3(c). The plastic deformation is the permanent distortion that occurred by the compressing, stretching or twisting during the compression testing and is not available. Their characteristics are similar to those of carbon steel as seen in Figure 2(b). The strain energy in steel conduits under compression force can be calculated by $U = V\sigma^2/2E$ when V defines as a volume of the body, σ is a strain and E is Young's modulus [22]. The strain energy is the energy stored by a sample undergoing deformation. The highest strain energy of 1092.71 Jmm^{-3} was obtained for steel wire thickness of 0.6 mm. This result shows that the thickness of steel wire directly affects the mechanical performance of spring steel conduit.

The simulation of the stress as a function of compression force and the measured yield stress are shown in Figure 4. Note that, yield stress is defined as a compression force at yield per cross-section area of the wire thickness. The yield stress relates to the stress at which sample changes from elastic deformation to plastic deformation. It can be seen that the measured yield stress was aligned on the simulation curves. The simulation was obtained using the compression force from 750 N to 2200 N. A linear relation is obtained between the stress (σ) and the compression force (F). The relationships are followed by $\sigma_{0.3mm} = 0.0687F$, $\sigma_{0.4mm} = 0.0640F$, $\sigma_{0.5mm} = 0.0618F$ and $\sigma_{0.6} = 0.0606F$.

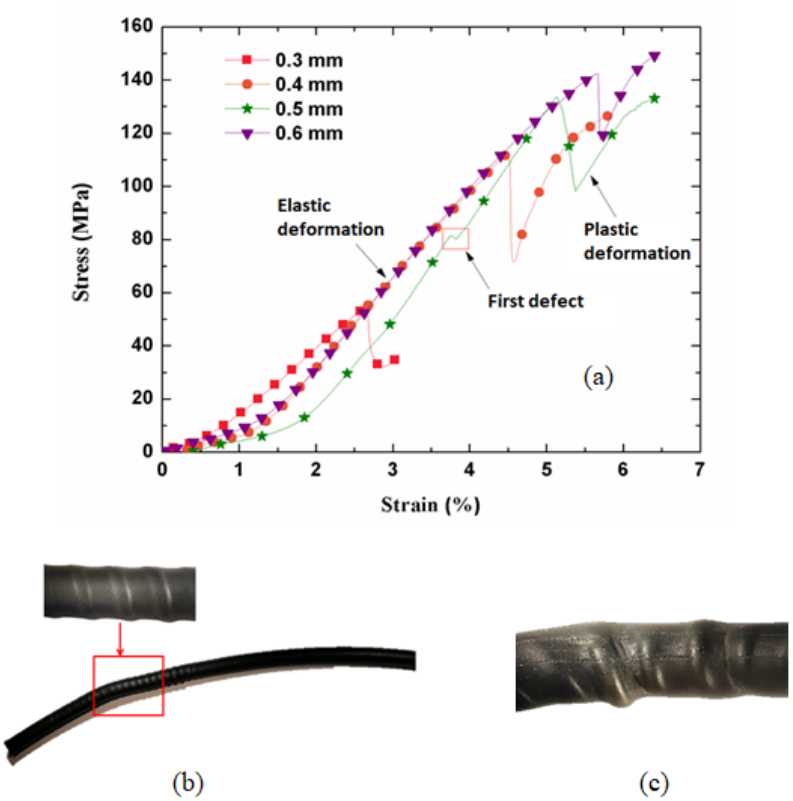

Figure 3. (a) Stress-strain curves with the different steel wire thickness (0.3 mm to 0.6 mm)
(b) First defect of 0.5 mm steel wire thickness
(c) Plastic deformation of 0.5 mm steel wire thickness

Table 4. Mechanical properties of spring steel conduit with different steel wire thicknesses.

Steel wire thickness (mm)	Elastic Modulus (MPa)	Stress at first defect (MPa)	Yield stress (MPa)
0.3	21.664	36.587	53.637
0.4	29.204	56.090	112.036
0.5	29.221	81.235	133.761
0.6	30.515	129.363	141.608

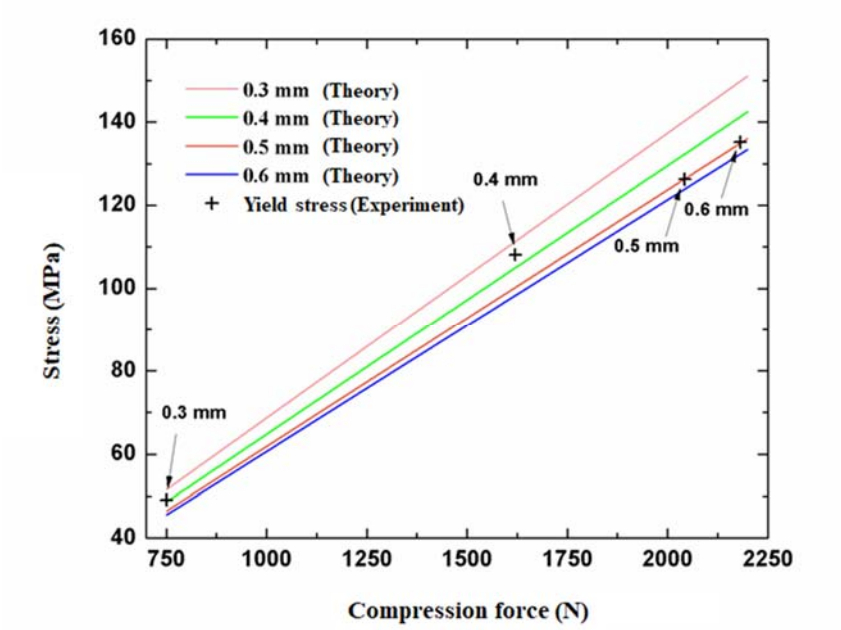

Figure 4. Comparison between theoretical and experimental results of yield stress as a function of compression force with four difference steel wire thickness between 0.3 mm to 0.6 mm.

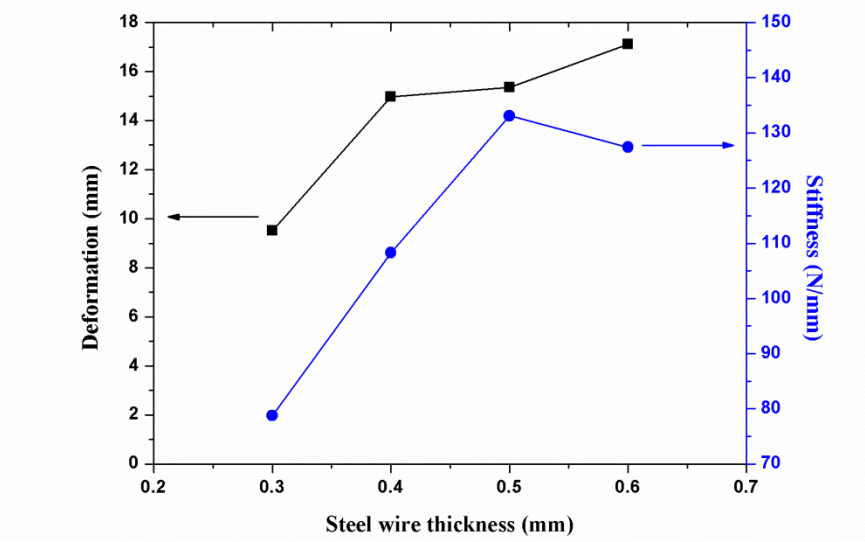

Figure 5. Deformation and stiffness as a function of steel wire thickness from 0.3 mm to 0.6 mm.

For the compression testing, the deformation behavior is proportional to the stress that applied within the elastic range of the material. It has begun to permanently deform and lose their functional working when it is out of range. For the spring steel conduit, the deformation is caused by the change of steel wire structure on the stages of damage in bending to broken. Thus, it can be clearly seen and calculated by the change of length of the spring steel conduit (ΔL). It is related to

the stiffness of the material structure. It is defined as the properties of a material which is rigid and difficult to bend under force enhancement. It can be returned to original shape once the load is removed. Stiffness (k) [23] is associated with elastic deformation following by

$$k = \frac{F_{\max}}{\Delta L}$$

where F_{max} is the maximum force (refer to the force at yield point).

The deformation and stiffness as a function of steel wire thickness are shown in Figure 5. The deformation and stiffness characteristics of the spring steel conduit were in the same manner. The deformation increases from 10 mm to 17 mm as the wire thickness increases from 0.3 to 0.6 mm. The stiffness increases from 78 N/mm to 132 N/mm as the wire thickness increases from 0.3 to 0.5 mm and then the stiffness slightly decreases to 128 N/mm at 0.6 mm. The stiffness is the ability of the sample to resist deformation. The high thickness of steel wire is needed in order to achieve the high stiffness of spring steel conduit and to avoid bends and deformation.

Figure 6 shows the safety factor and compression force at yield point as a function of steel wire thickness. It was found that the yield force increases from 750 to 2,181 N as the steel wire thickness increases from 0.3 to 0.6 mm, respectively. From JASO T 001-97 standard, the compression force must be at least 1,000 N and the safety factor of 1.5 is always taken. Generally, the increase in steel wire thickness resulted in a linear increase in yield stress. Both conditions are required in order to optimize the spring steel conduit. Thus, it does not signify with the steel wire thickness less than 0.4 mm due to the lower safety factor. Currently, the 0.6 mm of steel wire is also used in the control cable manufacturing. To provide the advantages of cost reduction, the steel wire thickness of 0.4 mm should be considered. It has a safety factor of 1.62 and compression force of 1,620 N that passed a standard design.

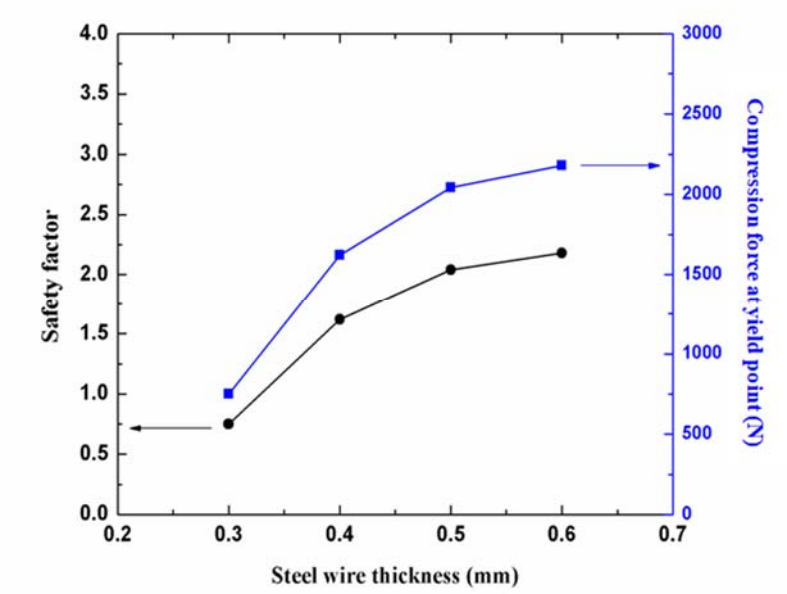

Figure 6. A safety factor and compression force as a function of steel wire thickness from 0.3 mm to 0.6 mm.

4. Conclusions

The mechanical characteristics of spring steel conduit was analysed by compression testing with the steel wire thickness varying from 0.3 mm to 0.6 mm and optimization under JASO T001-97 standard. Currently, the 0.6 mm of steel wire has also been used in the control cable manufacturing while the minimization of steel wire thickness of 0.4 mm was obtained. The mechanical parameters such as elastic modulus, first defect and yield stress were presented. The experimental results were compared with the theoretical calculation. The agreement between the two results confirms the validity of the compression testing.

5. Acknowledgements

The authors gratefully acknowledge the financial support provided to this research by Thai Steel Cable Public Company Limited and Industrial-University Collaborative Research Centre, College of Advanced Manufacturing Innovation, King Mongkut's Institute of Technology Ladkrabang.

References

[1] Buthgate, S., Saenthon, A. and Kaitwanidvilai, S. 2017. Development of new part of casing cap for the parking brake cable using finite element analysis. *International Journal of Innovative Computing, Information and Control*, 13, 659-670.
[2] JASO F903-75, 1975. Japanese Automobile Standard.
[3] Musikhin, V.A. 2006. Advantages of using steel cables. *Architecture, Construction*. 4-5, 38-40.
[4] Oller, S., Aramayo, S.A.O., Nallim, L.G. and Martinez, X. 2018. Composite Materials. In: I. Dincer, ed. *Comprehensive Energy Systems, Vol. 2, Energy Materials*. Amsterdam: Elsevier, pp. 235-265.
[5] Geiger, M., Kleiner, M., Eckstein, R., Tiesler, N. and Engel, U. 2001. Microforming. CIRP Annals, 50(2), 445−462.
[6] Kals, T.A. and Eckstein, R., 2000. Miniaturization in sheet metal working. *Journal of Materials Processing Technology*, 103(1), 95-101.
[7] Blumenschein, L. H., McDonald, C. G. and O'Malley, M. K. 2017. A cable-based series elastic actuator with conduit sensor for wearable exoskeletons. *IEEE International Conference on Robotics and Automation (ICRA)*, 6687-6693.
[8] JASO T001-97, 1997. Japanese Automobile Standard.
[9] Chou, T.-W. 1989. Flexible composites. *Journal of Materials Science,* 24, 761-783.
[10] Chou, T.-W. and Takahashi, K. 1987. Nonlinear Elastic Behaviour of Flexible Fibre Composites. *Composites*, 18, 25-34.
[11] Luo, S.Y. and Chou, T.-W. 1986. Modelling of the nonlinear elastic behaviour of elastomeric flexible composites. Paper presented at American Chemical Society Meeting, Anaheim, California, September 1986.
[12] Sumikawaa, S., Ishiwataria, A., Hiramotoa, J., Yoshidab, F., Clausmeyerc, T. and Tekkayac, A.M. 2017. Stress state dependency of unloading behavior in high strength steels. *International Conference on the Technology of Plasticity,* ICTP 2017, 17-22.
[13] Yoshida, F., Uemori, T., Fujiwara, K., 2002. Elastic–plastic behavior of steel sheets under in-plane cyclic tension-compression at large strain. *International Journal of Plasticity*, 18, 633-659.

[14] Luo, L., Ghosh, A.K., 2003. Elastic and inelastic recovery after plastic deformation of DQSK steel sheet. *Journal of Materials Processing Technolology,* 125, 237-246.
[15] Sun, L. and Wagoner, R.H., 2011. Complex unloading behavior: Nature of the deformation and its consistent constitutive representation. *International Journal of Plasticity*, 27, 1126-1144.
[16] Danpinid, A., Luo, J., Vappou, J., Terdtoon, P. and Konofagou, E. E. 2009. Characterization of the stress-strain relationship of the abdominal aortic wall in vivo. *2009 Annual International Conference of the IEEE Engineering in Medicine and Biology Society*, Minneapolis, 1960-1963.
[17] Luo, Y., Wang, Q. and Yang, B. 2011. Low cycle fatigue tests on low carbon steel. *2011 International Conference on Business Management and Electronic Information*, Guangzhou, 741-746.
[18] Nguyen, N.-V., Kim, J.J. and Kim, S.-E. 2018. Methodology to extract constitutive equation at a strain rate level fromindentation curves. *International Journal of Mechanical Sciences,* 152, 363-377.
[19] Sharpe, W.N., Yuan, B., Vaidyanathan, R. and Edwards, R.L. 1997. Measurements of Young's modulus, Poisson's ratio, and tensile strength of polysilicon. *Proceedings of IEEE. The Tenth Annual International Workshop on Micro Electro Mechanical Systems. An Investigation of Micro Structures, Sensors, Actuators, Machines and Robots*, Nagoya, Japan, 424-429.
[20] Cruz, S.A. and Zanin, M. 2004. Assessment of dielectric behavior of recycled/virgin high density polyethylene blends. *IEEE Transactions on Dielectrics and Electrical Insulation*11(5), 855-860.
[21] Heinrich, M., Sichting, F. and Kroll, L. 2012. Microinjection molding of polypropylene (PP) filled with MWCNT: Influence of processing parameters on the mechanical properties. *IEEE Nanotechnology Materials and Devices Conference (NMDC2012)*, 111-115.
[22] Case, J. and Chilver, A.H. 1959. Strain energy and complementary energy. *Strength of Material,* 18, 308-323.
[23] Benli, S., Aksoy, S., Havıtcıoglu, H. and Kucuk, M.. 2008. Evaluation of bone plate with low-stiffness material in terms of stress distribution. *Journal of Biomechanics*, 41, 3229-3335.

Influence of Maturity and Drying Temperature on Antioxidant Activity and Chemical Compositions in Ginger

Sirinapa Sida[1], Rajnibhas Sukeaw Samakradhamrongthai[2] and Niramon Utama-ang[1*]

[1]Division of Product Development Technology, Faculty of Agro-Industry,
Chiang Mai University, Chiang Mai, Thailand
[2]Department of Food Technology, Faculty Agro-Industry, Prince of Songkla University,
Hat Yai Campus, Songkla, Thailand

Received: 15 October 2018, Revised: 7 January 2019, Accepted: 14 February 2019

Abstract

The objective was to study the effect of maturity at harvest and drying temperature on antioxidant activity and physiochemical properties of ginger (*Zingiber officinale*). The effects of two different maturities of harvest, i.e. 6 months and 9 months were examined. It was found that the contents of carbohydrate and fiber values increased in the 9 month sample. The 9-month sample was higher in total phenolic contents (5.08 µmol Tannic acid/g), DPPH (85.33% inhibition), ABTS (42.23 µmol Trolox/g) and FRAP (13.78 µmol Trolox/g) than the younger 6-month sample. In essential oil constituents, the 9-month sample contained higher amounts of geranial (28.31%), neral (15.29%), β-phellandrene (13.32%), campene (7.77%) and α–zingiberene (6.17%) in comparison to the 6month samples. The 9-month sample contained the highest level of 6-gingerol (24.36 mg/g). Therefore, the ginger harvested at 9 months was selected for the study of different drying temperatures. Drying times and temperature to achieve moisture content below 10% at 308 min, 60°C were proven to be the best condition as it achieved the highest total phenolic content (12.21 µmol Tannic acid /g), DPPH (91.35%), ABTS (223.50 µmol Trolox/g) and FRAP (42.39 µmol Trolox/g). Ginger contains 45 volatile compounds and the highest main compounds being αzingiberene (18.28%), α-farnesene (10.73%) and geranial (12.42%) when drying temperature was at 60°C. The content of 6-gingerol was also found to be the highest in the sample dried at 60°C (12.57 mg/g).

Keywords: *Zingiber officinale*, ginger, maturity, antioxidant, volatile compounds, drying
DOI 10.14456/cast.2019.4

1. Introduction

Ginger (*Zingiber officinale* Roscoe) is a unique aromatic herb used around the world in food and spices. It contains both non-volatile and volatile compounds. The unique aroma is provided by the

*Corresponding author: Tel.: 66 53 948284 Fax: 66 53 948214
E-mail: niramon.u@cmu.ac.th

essential oils and the pungency contained in the non-volatile compounds. The odor of ginger depends on its major volatile oil, the content of which changes 1-3%. More than 50 volatile compounds were found and characterized in ginger by using gas chromatography mass-spectrometry. The essential oil contains monoterpenoid and sesquiterpene hydrocarbons. The monoterpenoids include β-phellandrene, camphene, cineole, geraniol, citral, terpineol and borneol. The sesquiterpenoids include α-zingiberene, β-sesquiphellandrene, β-bisabolene, (E,E)-α-farnesene, ar-curcumene and zingiborol [1]. Ginger also contains a variety of oleoresins, namely gingerol, shogaol, paradol and zingerone. Gingerol is the rhizome compound responsible for pungency. Gingerol compounds are transformed at high temperatures to shogaol [2]. Period from planting to maturity could affect the antioxidant activities and bioactive compounds. The main bioactive compounds of Jamaica ginger harvested at 6-8 months after planting depend on the variety of location and the age of rhizome [3] and the harvest duration depends on the end-use. In Thailand, there are no studies on the proximate, essential oil composition and bioactive compounds of fresh ginger cultivars of 6- and 9- month maturity period. Generally, fresh ginger consists of 85-95% moisture content and is easily affected by microbial spoilage and chemical decomposition. The drying method reduces the moisture content resulting in bacterial growth inhibition and delays deteriorative biochemical reactions. However, the drying temperature can cause deterioration of the physical and chemical properties and some of the oil constituents were also changed to less volatile compounds. The other researchers reported that the antioxidant activity showed highest activity in 80% methanolic ginger extract because it is suitable extracting solvent capable of extracting the lipophilic antioxidant composites [4]. Therefore, the purpose of this study is to investigate the effects of maturity at harvest and drying temperature on physical, chemical and essential oil composition of ginger. In addition, the total phenolic contents, antioxidant properties (DPPH, ABTS and FRAP), essential oil compositions and main bioactive compounds were also measured.

2. Materials and Methods

2.1 Raw materials

The ginger rhizomes (*Zingiber offinale* Roscoe) were divided into two groups according to their maturity (6 months and 9 months). These ginger rhizomes were obtained from the same source in Chiang Rai, Thailand.

2.2 Effects of physiochemical properties of different maturity

The peeled gingers (6 months and 9 months) were washed in distilled water and cut into 0.2 x 4 x 0.4 cm. The fresh ginger was then kept in the vacuum package and stored in refrigerator at 0-4 °C (Mitsubishi electric, MRFV 22M/BR, Japan) for 24 h before further analysis.

2.3 Effects of physicochemical properties of different drying temperatures

The drying process was as per the method reported earlier with some modifications [5]. Samples were spread in the hot air dryer (Armfield, Hamshire, England). Drying experiments were performed with a sample of 200 g for ginger rhizomes dried in a thin layer at 40, 50 and 60°C. The moisture content was evaluated every 30 min to monitor the moisture loss. The weight loss of the sample was recorded every 10 min using a data logger (DT 800, Data taker, Scoresby, Victoria, Australia). The drying was finished when the weight was stable and the moisture content of the ginger had been decreased to 10% wet basis. The dried ginger was ground, sieved at 1.2 mm, kept

in the vacuum aluminum foil package and stored in a desiccator at ambient temperature for at least 24 h before further analysis.

2.4 Physical characteristics and proximate analysis

The color was expressed in L*, a*, b* by the colorimeter (Konica Minolta CR-400 Series, Japan). Water activity was measured using an AquaLab Water Activity Meter (Decagon, USA). Proximate analysis was determined by using standard AOAC methods [6].

2.5 Total phenolic content (TPC)

Ten grams of ground fresh ginger was accurately weighed and transferred into 100 ml of 80% methanol [4]. The sample was shaken for 3 h at an ambient temperature. Following this technique, it was centrifuged at 4,000 rpm for 20 min and then filtrated through Whatman No. 1 paper. Then the ginger extracts were used in total phenolic compound analysis and antioxidant activities (DPPH, ABTS and FRAP). Total phenolic compounds were examined using the method described by Re *et al.* [7]. The ginger solution (200 µl) and 10% Folin-Ciocalteu reagent (1 ml) (Loba chemie, India) were mixed and 2% Na_2CO_3 was then added with a water:methanol (4:6) diluting solvent to make a total volume of 10 ml. Absorbance was recorded at 740 nm after 30 min using a spectrophotometer (UV-Vis model 1601, Shimadzu, Japan). The absorbance was then compared with the tannic acid standard curve. The result was shown as µmol per gram of dried weight.

2.6 Antioxidant activities

2.6.1 DPPH radical-scavenging activity

Free radical scavenging activity of the extracts was determined using stable free radical 2, 2-Diphenyl-picrylhydrazyl (DPPH) (Sigma-aldrich, U.S.A.) with some modifications [4]. Four ml of extract solution and 1 ml of DPPH solution were mixed (0.1 mM in methanol) by a vortex mixer and then stood at room temperature in dark storage for 30 min. The absorbance was recorded at 520 nm. The percentage of scavenging effect was calculated using the following equation (1) shown below:

$$\text{Radical scavenging activity (\%)} = [A_0 - A_1]/A_0 \times 100 \quad (1)$$

Where A_0 was the absorbance of control solution (DPPH without sample) and A_1 was the absorbance of the ginger extract in DPPH solution.

2.6.2 ABTS method

Antioxidant activity was evaluated using 2, 2′-azinobis (3-ethylbenzothiazoline-6-sulphonic acid) diammonium salt (ABTS) (Fluka, Germany) according to the modified method from Re *et al.* [7]. A mixture between 7 mM ABTS and 2.45 mM potassium persulphate, the ABTS•+ solution, was stood in dark place for 14±2 h before use. Afterwards, the ABTS•+ solution was diluted with ethanol to measure an absorbance of 0.700 ± 0.02 at 734 nm. Ginger extract (150 µl) was allowed to react with 4,850 µl of the ABTS•+ solution for 6 min and then read by a spectrophotometer at 734 nm. The absorbance was compared with the Trolox standard curve and the results are shown in µmol per gram dry weight.

2.6.3 Ferric reducing ability power assay (FRAP assay)

The FRAP assay was determined by the modification method from Benzie and Strain [8]. The FRAP reagent, consisting of 300 mM acetate buffer (1.22 g $C_2H_3NaO_2 \cdot 3H_2O$ and 8.05 ml $C_2H_4O_2$), pH 3.6, 10 mM TPTZ (2, 4, 6-tripyridyl-s-triazine) solution in 40 mM HCl, and 20 mM $FeCl_3 \cdot 6H_2O$ solution in the ratio of 10: 1: 1, was warmed at 37 ºC before use. The FRAP solution (3 ml) was added to 150 µl of ginger extract for 10 min at 37 ºC and the absorbance was recorded at 593 nm. The results are shown as µmol per gram dry weight.

2.7 Analysis of volatile compounds from essential oil in ginger using gas chromatography

The volatile compounds from essential oil in ginger were studied using gas chromatography according to the method modified from Kiran *et al.* [1]. Peeled fresh rhizomes were chopped and approximately 200 g (30 g for ground dried ginger) of this material was hydrodistilled for 3 h. The essential oil was kept in micro tubes and frozen at -20 ºC. Prior to analysis, the extracts were dissolved with hexane at appropriate concentration and filtered by 0.45 µm. pore size filter before being measured by the gas chromatography-mass spectrometry (GC-MS) and gas chromatography (GC-FID).

Essential oils were studied using Shimadzu GC-MS model GC-17A and equipped with mass spectrophotometer model GC-MS QP 5050A. The carrier gas was helium at a flow rate of 1 ml/min using capillary column (BPX-5, SGE, Ltd., Melbourne, Victoria, Australia) which had a dimension of 30 m × 0.250 mm inner diameter × 1.00 µm for this analysis. A split ratio of 1:50 was used. The oven temperature was set from 80°C (holding time of 1 min) to 220°C at 5 °C/min and held for 10 min. The injection port was heated to 250°C. The interface of temperature was 270°C with an ionization voltage of 70 eV. The constituents were identified by comparison with authentic standards, retention indices (RIs) and mass spectra (MS) of National Institute of Standards and Technology (NIST) sources, flavors and fragrance of natural and synthetic compounds (FFNSC) references.

Essential oils were studied using a gas chromatograph model Shimadzu GC-2010. Helium was used as the carrier gas at a flow rate of 1 ml/ min. A capillary column (60 m × 0.22 mm inner diameter × 1.00 µm df) was used for the analysis (BPX- 5, SGE, Ltd., Melbourne, Victoria, Australia), and a flame ionization detector (FID) was used. A split ratio of 1:50 was used. The oven temperature was started at 80°C and held for 1 min before heating to 220°C at a rate of 5°C/min and held for 10 min. The injection port was heated to 250°C, and the detector temperature was set at 300°C. Identification of compound was calculated by retention indices using a C_8-C_{20} alkane standard solution.

2.8 Analysis of active compounds in ginger using high performance liquid chromatography method (HPLC)

Ground ginger (10 g) was weighed and extracted with 100 ml of 95% ethanol by electronic shaker for 30 min. The solvent was concentrated in a rotary evaporator and filtered through a Whatman No.1. After filtering through a 0.2 µm syringe filter, the final sample was used for injection. Standards of 6- gingerol, 6- shogaol, paradol and zingerone were prepared. The method was performed on HPLC (HPLC, Agilent Technologies, Santa Clara, CA, USA) with a photodiode-array detector. The optimal HPLC system contained a C_{18} reverse phase column (Water C_{18}, 250x4.6 mm i.d., 5 µm particle size). The gradient elution was acetonitrile and water at a flow rate of 1.0 ml/min and a detection of 282 nm. The mobile phase contained water (A) and acetonitrile (B). Both solutions were filtered by 0.45 µm pore size filter. The gradient elution program was set as follows:

from 0 to 25 min, B was isocratic at 33%; from 25-35 min, solution B was changed from 33% to 55%; from 35 to 60 min, B followed changed linearly from 55% to 90%; from 60 to 65 min, B was a linear change from 90% to 33%; and from 65 to 70 min, B was isocratic at 33% [9].

2.9 Statistical analysis

The data was shown as mean±standard deviation for at least triplicate analyses. Mean comparisons of physical and chemical properties (proximate analysis, total phenolic content, DPPH, ABTS, FRAP and bioactive compounds) were analyzed using ANOVA for a Completely Randomized Design (CRD) in SPSS version 17.0 (SPSS Inc., Chicago, USA). Statistical significance was analyzed for $p \leq 0.05$ using Duncan's New Multiple Range Test (DMRT).

3. Results and Discussion

3.1 Effects of 6 and 9-month maturity on the physiochemical properties of ginger rhizome cultivars

The physicochemical properties of ginger harvested at different maturities are shown in Table 1. The different harvest time of the ginger rhizome affected the color (L*, a* and b*), moisture content, water activity, carbohydrate, protein, fat, fiber and ash. The color of the ginger indicated a light yellow trend. The L* movement showed lightness and b* direction denoted a change to yellow. Ginger harvested at 9 months had higher yellow and lightness than the 6-month samples. The ginger harvested at 6 months had higher moisture content and water activity than the samples at 9 months. There was also significant change in crude fiber as their composition increased in the more mature sample. Harvest for dried herbs and essential oil is best at long maturity with increase of the fiber content [10]. The carbohydrate content increased from 31.36% (6-month sample) to 39.09% (9-month sample). The fiber content increased from 38.41% (6-month sample) to 43.73% (9-month sample). However, the protein, fat and ash contents of the sample were decreased in the more mature ginger. Increase of crude fiber and decrease of fat and protein contents of rhizome were observed after 6 months and 15 days [11]. Other researchers found that dry recovery, carbohydrate and crude fiber were positively correlated with maturity whereas essential oil, oleoresin and protein were negatively related with maturity [12, 13]. The values for composition of ginger are reported in the following range: 7.2 to 8.7, 5.5 to 7.3 and 2.5 to 5.7 g/100 g dried weight for protein, fat and ash, respectively [1]. Our study showed that ginger harvested at 9 months contained a higher total phenolic content (TPC) (5.08±0.28 µmol tannic acid/g) than ginger harvested at 6 months (2.61±0.12 µmol tannic acid/g) (Table 1). This finding is in an agreement with Chumroenphat *et al*. [14] who reported that matured ginger had a higher total phenolic content than immature ginger. Antioxidant activities of plant extracts were usually correlated to their phenolic content. Hydrogen donating characteristics of the phenol compounds can inhibit free radical induced to scavenge free radicals and donate oxygen [1]. However, it is known that non phenolic antioxidants might also lead to the antioxidant activity of plant extract [15, 16]. Ginger harvested at 9 months was able to reduce the stable free radical 2, 2- diphenyl-1-picrylhydrazyl (DPPH) to yellow-colored DPPH (70.48%). DPPH radical scavenging activity in ginger harvested at 9 months was found to be 70.48%, compared to 55.40% found in ginger harvested at 6 months. In addition, the ginger harvested at 9 months also displayed the highest radical scavenging potential of ABTS (42.23±7.80 µmol Trolox/g) and FRAP (13.78±0.66 µmol Trolox/g). According to Chen *et al*. [17], DPPH values of methanolic extract were found between 32% and 90.1% of 18 different ginger types.

Table 1. Physicochemical properties of fresh ginger at different maturities.

Characteristics	6-month maturity	9-month maturity
L*	55.40 ± 0.01^{b}	70.48 ± 0.06^{a}
a*	7.29 ± 0.31^{a}	-1.54 ± 0.90^{b}
b*	9.39 ± 0.18^{b}	23.21 ± 3.76^{a}
Water activity	1.000 ± 0.01^{a}	0.996 ± 0.01^{b}
Moisture (% wet basis)	94.88 ± 0.15^{a}	87.25 ± 1.03^{b}
Carbohydrate (% dry basis)	31.36 ± 0.98^{b}	39.09 ± 0.58^{a}
Protein (%dry basis)	11.60 ± 0.37^{a}	8.95 ± 0.71^{b}
Fat (%dry basis)	4.27 ± 0.20^{a}	2.33 ± 0.11^{b}
Fiber (%dry basis)	38.41 ± 0.41^{b}	43.73 ± 0.64^{a}
Ash (%dry basis)	14.35 ± 0.82^{a}	6.63 ± 0.13^{b}
Total Phenolic content (μmol Tannic acid/g)	2.61 ± 0.12^{b}	5.08 ± 0.28^{a}
DPPH (%inhibition)	62.97 ± 1.49^{b}	85.33 ± 2.47^{a}
ABTS (μmol Trolox/g)	7.57 ± 3.03^{b}	42.23 ± 7.80^{a}
FRAP (μmol Trolox/g)	8.40 ± 0.59^{b}	13.78 ± 0.66^{a}

$^{a-b}$ Different letters show significant difference between means in the same row ($p \leq 0.05$).

Essential oil composition is one significant parameter to determine variation among different ginger cultivars. By GC-MS and GC-FID analyses and it was found that there were 44 volatile compounds in the essential oil of ginger cultivars. The percentage compositions of various components from ginger after planting at 6 and 9 months are shown in Table 2. The data shows that there are 34 and 36 volatile compounds in ginger harvested at 6 and 9 months, respectively. The data clearly reports a difference in essential oil composition with different maturity periods. The major volatile compounds of 6-month cultivars are geranial (24.20%), nerol (13.34%), 3-carene (10.53%), β-phellandrene (10.25%), campene (6.08%) and α-zingiberene (4.32%). The main volatile compounds of 9-month cultivars are geranial (28.31%), neral (15.29%), β-phellandrene (13.32%), campene (7.77%), α-zingiberene (6.17%) and α-pinene (3.47%). A higher undecanone concentration (0.27%) was found in 6-month cultivars when compared to 9-month cultivars (0.17%) which is in an agreement with previous research [1]. Ginger essential oil was also shown to be a combination of sesquiterpenic compounds that contain α–zingiberene, β-sesquiphellandrene, neral and geranial as well as monoterpenoid compounds with camphene, geranial and geranyl acetate as main constituents [2]. Ginger harvested at 6 months and 9 months showed higher monoterpene content than sesquiterpene content. The data clearly shows ginger harvested at 9 months has more main volatile compounds than at 6 months. Higher contents of geranial (28.31%), neral (15.29%), β-phellandrene (13.32%), campene (7.77%), α-zingiberene (6.17%), α-farnesene (3.30%), β-sesquiphellandrene (2.72%) and ar-curcumene (1.94%) were found in ginger harvested at 9 months in comparison to the ginger harvested at 6 months. The low molecular weight of monoterpenes:

Table 2. Essential oil composition of ginger cultivars harvested at 6-month and 9-month maturity using GC-MS and GC-FID.

No.	Compound	Composition (%)		RI[a]	Identification
		6-month maturity	9-month maturity		
1	tricyclene	0.09	0.16	927	RI
2	α- pinene	3.16	3.47	938	RI
3	camphene	6.08	7.77	951	RI
4	4-carene	-	0.12	-	MS[b]
5	β- pinene	0.54	0.59	976	RI
6	myrcene	3.26	3.17	990	RI, MS
7	α- phellandrene	0.36	0.46	1007	RI, MS
8	β-phellandrene	10.25	13.32	1032	RI
9	cineole	0.28	-	1034	RI
10	2-cymanene	0.61	-	1086	RI
11	2-nonanone	3.93	1.59	1093	RI
12	3,3-dimethyl-1octene	0.18	0.20	1151	RI, MS
13	citronellal	-	0.85	1154	RI, MS
14	iso borneol	0.44	-	1162	RI
15	borneol	0.33	0.11	1162	RI, MS
16	α -terpineol	0.89	0.81	1189	RI, MS
17	citronellol	0.66	0.96	1229	RI, MS
18	neral	7.65	15.29	1226	RI, MS
19	3-carene	10.53	-	-	MS
20	nerol	13.34	2.58	1255	RI, MS
21	bornyl acetate	0.16	0.16	1272	RI, MS
22	2-undecanone	0.27	0.17	1285	RI, MS
23	citronellyl propionate	0.99	-	1255	RI, MS
24	geranial	24.20	28.31	1272	RI, MS
25	β- elemene	-	0.22	1337	RI
26	citronellyl acetate	-	1.66	1358	RI
27	copaene	-	0.08	1388	RI
28	geranyl acetate	-	0.51	1381	RI
29	ar-curcumene	0.95	1.94	1393	RI, MS

Table 2. (cont.)

30	chamigrene	0.36	0.15	1478	RI
31	zingiberene	4.32	6.17	1487	RI, MS
32	e-e-α- farnesene	2.39	3.30	1494	RI
33	γ-cadinene	-	0.18	1514	RI
34	β -sesquiphellandrene	1.31	2.72	1507	RI
35	selina-3,7(11)-diene	0.14	-	1384	RI
36	trans-cadinene ether	0.09	-	1400	RI
37	hexadecane	0.50	-	1447	RI
38	β-bisabolene	0.15	1.33	1456	
39	γ-elemene	-	0.14	1586	RI
40	β-gurjunene	-	0.12	1596	RI, MS
41	β-cadin-4-en-10-ol	0.53	0.14	1627	RI, MS
42	caryophyllene	0.17	0.57	1638	RI, MS
43	β-eudesmol	-	0.61	1662	RI, MS
44	trans-α-bergamotene	0.54	0.16	1693	RI, MS

[a]Retention indices, [b]mass spectral data.

α-pinene, cineole, borneol, neral and geranial are shown in various proportions leading to aroma characteristics in the products. For instance, citral with its two isomers neral and geranial, was found high (between 6.6-20.7% citral) in different areas of Brazilian-grow cultivars while it was found only 1.9-4.3% in Chinese cultivars [19]. Australian oils also had high citral content (27%) with an average of 19% [20, 21]. The citral content affecting the lemony odor of ginger is popularly used in the food manufacturing [22]. In summary, the citral content increased with the age of rhizomes and is higher than zingiberene at 9-month maturity. These data indicated that the volatile compounds of each cultivated ginger depend on the age of rhizome, environmental origin, and climate surroundings. Cultivars of ginger at 9 months contained significantly higher concentrations of volatile compounds than 6-month cultivars and duration of 8-9 months is suitable for essential oil production [10].

Our HPLC method allows the finding of all four ginger's pungency at both maturity periods (Figure 1). The content of 6-gingerol increased with the age of the rhizome significantly ($p \leq 0.05$). The content in 9-month sample (24.36±0.56 mg/g) was higher than the 6-month sample (21.55±2.80 mg/g). This suggests that manufacturers should purchase ginger rhizome with higher level of 6-gingerol throughout the growth period. However, the previous research found that 6-gingerol content directly associated with oleoresins amounts and reduced by the effects of long term planting with an exception in some locations [1]. In Hawaii, 6-gingerol in rhizomes increased over period examined, while it reached a peak at 4 months on a dry matter after planting, then decreased and increased again to reach a second peak at 6 months [23]. Similarly, the maximum oleoresin content was reached after 7 months. Time from planting to maturity may be highly affected by the type of soil [24]. High levels of 6-shogoal were detected in 6-month samples (9.02±1.01 mg/g) compared to low levels in 9-month samples (5.59±0.09 mg/g). Shogaol is often found at low

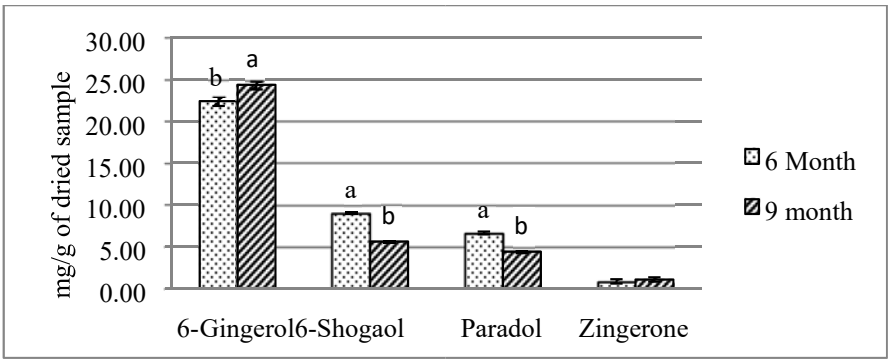

Figure 1. Variations in 6-gingerol, 6-shogaol, paradol and zingerone contents of ginger during maturation (6 and 9 months).

concentration in fresh ginger during long term storage of dried ginger [14]. The 6-month samples contained higher levels of paradol (6.62±0.07 mg/g) than the 9-month samples (4.38±0.16 mg/g). Zingerone is found in low level in fresh ginger and is also produced from gingerol during the process; this compound is less pungent and has a spicy aroma [25]. Contents of zingerone observed in the samples were not significantly different in both maturations. In summary, fiber and the levels of volatile compound and bioactive compound are the most main criteria for the determination of suitable ginger rhizomes for production [26]. The best time to harvest ginger for the extracts of high quality is 9 months. By allowing for a longer harvesting time, it will ensure maximum returns for manufacturers. Therefore, we selected 9 -month maturity ginger for further investigation because the unique aroma of this cultivar comprises significantly higher levels of pungent 6-gingerol, which create commercial interest of aroma ingredients [27].

3.2 Effects of physicochemical properties of different drying temperatures

The drying curves of ginger using a tray dryer to achieve moisture content of 10% are shown in Figure 2. Drying times to achieve moisture content below 10% were 510, 394 and 308 min for 40°C, 50°C and 60°C, respectively. The experimental results showed that drying at high temperature decreased the moisture content faster than at low temperature, resulting in shorter drying time.

From Table 3, both L*(brightness/darkness) and b*(yellowness/blueness) values were affected by thermal treatment. With high temperature the ginger turned darker with a slight yellowness with lower L* and higher b* because the browning of the ginger was greater at a higher drying temperature [5]. The color changes caused by heat processing may have affected the nonenzymatic browning of food and the deterioration of pigment in the food [28]. The proximate compositions of the sample studied are also presented in Table 3. The dried ginger exhibited water activity between 0.307-0.387 which was in an alignment with dried food specifications (a_w<0.6). The moisture content of the dried ginger ranged between 7.01-8.39% (wet basis) conforms to Thai agricultural standards of dried ginger powder which is limited to 10% [29]. Furthermore, there were no significant changes in the composition of carbohydrate (73.16-73.93%), protein (9.509.53%), fat (2.22-2.25%) and fiber (9.11-9.13%) after drying temperature was increased. The ash content decreased significantly ($p \leq 0.05$) from ginger subjected to higher temperature drying, which reduce the micronutrients represented in the investigation of the ash [30]. The previous reported

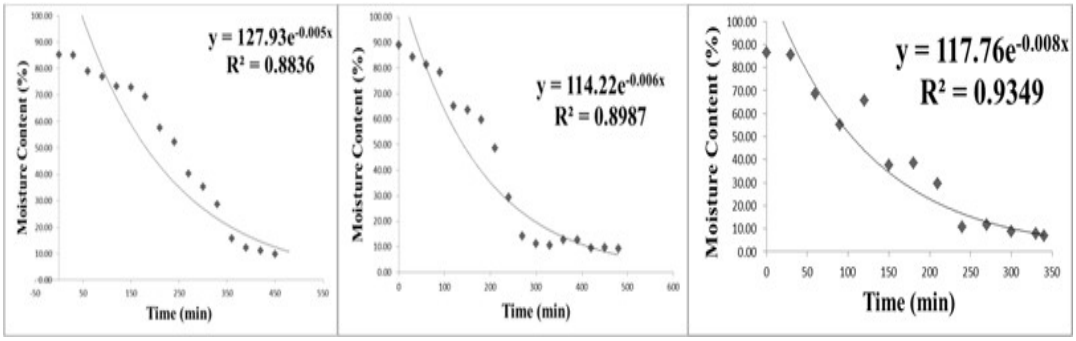

(a) 40°C (b) 50°C (c) 60°C

Figure 2. Drying time of ginger at different temperatures (a) 40°C (b) 50°C (c) 60°C.

Table 3. Physicochemical properties of dried ginger at different drying temperatures.

Characteristics	Drying Temperature (°C)		
	40	50	60
L*	81.23 ± 0.25^{a}	78.03 ± 1.81^{b}	75.15 ± 1.46^{c}
a*^{ns}	3.53 ± 0.85	2.19 ± 0.49	2.89 ± 0.57
b*	15.65 ± 0.12^{c}	21.61 ± 1.22^{b}	24.53 ± 1.10^{a}
Water activity	0.387 ± 0.027^{a}	0.378 ± 0.031^{a}	0.307 ± 0.014^{b}
Moisture (%wet basis)	8.39 ± 0.92^{a}	8.13 ± 0.39^{ab}	7.01 ± 0.10^{b}
Carbohydrate (%dry basis)^{ns}	73.16 ± 0.72	73.38 ± 0.49	73.93 ± 0.74
Protein (%dry basis)^{ns}	9.51 ± 0.27	9.50 ± 0.15	9.53 ± 0.26
Fat (%dry basis)^{ns}	2.25 ± 0.22	2.22 ± 0.06	2.23 ± 0.16
Fiber (%dry basis)^{ns}	9.11 ± 0.38	9.14 ± 0.33	9.13 ± 0.20
Ash (%dry basis)	5.96 ± 0.17^{a}	5.75 ± 0.07^{b}	5.19 ± 0.20^{b}
Phenolic content (µmol Tannic acid/g)	9.66 ± 1.01^{b}	10.34 ± 0.94^{b}	12.21 ± 0.22^{a}
DPPH (%inhibition)^{ns}	92.07 ± 0.54	92.02 ± 0.54	91.35 ± 0.50
ABTS (µmol Trolox/g)	134.80 ± 22.80^{c}	127.35 ± 5.13^{b}	223.50 ± 18.81^{a}
FRAP (µmol Trolox/g)	35.30 ± 2.70^{b}	23.64 ± 0.86^{c}	42.39 ± 0.78^{a}

$^{a-c}$ Different letters mean significant difference between means in the same row **(**DMRT, p≤ 0.05**).**
^{ns} letters show non-significant difference between means in the same row **(**DMRT, p>0.05**).**

values for composition of ginger (dry weight basis) were 72.84% for carbohydrate, 6.58% for protein, 5.53% for fat, 6.40% for ash and 8.30% for fiber [31]. In the present report, protein and fat contents were slightly changed from previous research.

The highest total phenolic content was observed in drying at 60°C (12.21±0.22 µmol tannic acid/g dry basis) and the lowest was observed in drying at 40°C (9.66±1.01 µmol tannic acid/g dry basis). This can be explained by the rehydration process causing the release of phenols from the cell walls and an increase in free hydroxyphenols and the transformation of new composites such as shogaol and zingerone [32]. For optimal phenolic content, shorter time at higher drying temperatures is required while the total phenolic content and antioxidant activities of ginger rhizomes were higher when drying was done at higher temperatures [14]. The DPPH radical inhibition (%) was not different among variables drying temperatures. The values of %inhibition ranged between 91.3592.07%. The ABTS and FRAP radical scavenging activities of ginger slices gave direct effect on total phenolic content. The highest ABTS was observed in drying at 60°C (223.50±18.81 µmol Trolox/g) and was the lowest when observed in drying at 40°C (134.80±22.80 µmol Trolox/g) and at 50°C (127.35±5.13 µmol Trolox/g). For FRAP values at 60°C (42.39±0.78 µmol Trolox/g) showed significantly ($p \leq 0.05$) higher than at 40°C and 50°C. It was observed that drying at various temperatures did not affect the DPPH radical inhibition (%) but rather influenced total phenolic content, ABTS and FRAP in this experiment. Therefore, the highest temperature (60°C) measured can be the most visible since it decreases the time and the costs of processing, resulting in higher total phenolic content and antioxidant activities than other temperatures (40 and 50°C). The usage of high temperatures in extraction and food storage leads to the damage of total phenolic content. However, significant changes were confirmed between the different temperatures and the use of lower temperatures caused a slower loss of antioxidant activities [30]. Some researcher reported that the drying temperature in the range of 60-80°C had no effect on total phenolic content, DPPH and ABTS scavenging inhibitions [33].

In the analysis of volatile compounds of ginger, 63 compounds are identified by GC-MS and GC-FID. The high contents of zingiberene, geranial, β-sesquiphellandrene and ar-curcumene comprise the important aromas of ginger [18]. Different drying temperature caused variations of volatile compounds. In drying at 60°C, 45 compounds were found and the main compounds were α-zingiberene (18.28%), geranial (12.42%), α-farnasene (10.79%), β-sesquiphellandrene (8.61%), neral (8.58%), ar-curcumene (6.09%). In drying at 60°C, zingiberene, α- farnasene, β-sesquiphellandrene, ar-curcumene and β-bisabolene were more prevalent in comparison to other dried samples. It was found that drying at 60°C conserved better levels of sesquiterpenes (zingiberene, farnesene, curcumene, β-sesquiphellandrene and β-bisabolene) while 44 and 46 compounds were detected when drying at 40°C and 50°C, respectively. This indicates that lower temperatures slightly decreased some sesquiterpenes and increased monoterphenes (campene, myrcrene, borneol, neral and geranial). The most geranial contents were found when drying at 50°C. Generally, the mild drying temperature had less effect on the volatile compounds despite its long treatment period whereas the strong drying process exerted significant effect on volatile compounds [34].

The 6-gingerol content was studied with several drying temperatures and the data are presented in Figure 3. The content of 6-gingerol increased as the drying temperature increased. The highest 6-gingerol content was found with drying at 60ºC. It was previously assumed that the high temperature and long exposure to heat would accelerate the deterioration and change of 6-gingerol [34]. In the previous research, 6-gingerol seems to decompose as the drying temperature increased to 60ºC [35] and transforms into 8-gingerol and 10-gingerol. Another research studied the effect of drying ginger rhizome on 6-gingerol contents and found that a long drying time can reduce the amount of this compound [36]. The 6-shogaol content ranged from 2.28 to 2.54 mg/g and is similar to the results from previous report (about 2-2.5 mg/g in ethanolic extract) [21]. Drying temperature of ginger directly affects the yield of 6-shogaol. The content of 6-shogaol slightly decreased as the

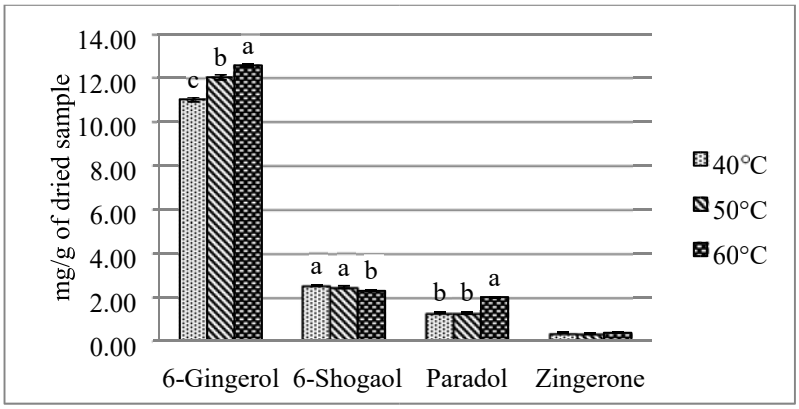

Figure 3. Variations in 6-gingerol, 6-shogaol, paradol and zingerone contents of ginger after drying at 40 ºC, 50 ºC and 60 ºC.

temperature increased (60ºC). Various drying temperatures have been tested to obtain different bioactive compounds such as paradol. Paradol contents tended to increase at the drying temperature of 60ºC (2.00±0.01 mg/g). Zingerone was much more stable than other active compounds during drying and the minimal content ranged from 0.35 to 0.38 mg/g in ginger.

4. Conclusions

In this paper, age and drying temperature were examined as they relate to the physical properties, proximate compositions, total polyphenol contents, antioxidant properties, essential oil compositions and bioactive compounds of ginger. The results found that the main volatile compounds of 9-month ginger were geranial, neral, β-phellandrene, campene, α–zingiberene, α-farnesene. Maximum content of 6-gingerol can be achieved with ginger at 9-month maturation. The optimal drying temperature at 60°C for 308 min in hot air dryer results in a sample rich in phenolic compounds with strong antioxidant. Our findings reveal that shorter drying time conserved major volatile compounds. The major volatile compounds were α-zingiberene, geranial, α-farnasene, β-sesquiphellandrene, neral and ar-curcumene when drying at 60°C. Drying temperature at 60°C gave the highest 6- gingerol content. To produce ginger powder, using ginger which has 9- months of maturation before drying at a temperature of 60ºC is recommended.

5. Acknowledgments

The raw materials for this research was provided by Hsu Chuan Foods CO., Ltd. (Chiang Rai, Thailand). Financially support was provided by Research and Researchers for Industries Scholarship (RRI, code MSD59I0047) under the Thailand Research Fund (TRF).

References

[1] Kiran, C.R., Chakka, A. K., Padmakumari, A., Menon, A.N., Kumar, M.M.S. and Venogopalan, V.V., 2013. Influence of cultivar and maturity at harvest on the essential oil composition, oleoresin and [6]-gingerol content from Northeast India. *Journal of Agricultural and Food Chemistry*, 61, 4145-4154.

[2] Semwal, R.B., Semwal, D.K., Combrinck, S. and Viljoen, AM., 2015. Gingerols and shogaols: Important nutraceutical principles from ginger. *Journal of Phytochemistry*, 117, 554-568.

[3] Bailey-shaw, Y., Williams, L., Jonor, G., Green, C., Hibbert, S., Salmon, C. and Ann marie, S., 2008. Changes in the contents of oleoresin and pungent bioactive principles of Jamaican ginger (*Zingiber officinale* Roscoe.) during maturation. *Journal of Agricultural and Food Chemistry*, 56, 5564-5571.

[4] Shirin, AP. and Jamuna, P., 2010. Chemical composition and antioxidant properties of ginger root (*Zingiber officinale*). *Journal of Medicinal Plants Research*, 4, 2674-2679.

[5] Phoungchandang, S., Nongsang, S. and Sanchai, P., 2009. The development of ginger drying using tray drying, heat pump-dehumidified drying, and mixed-mode solar drying. *Journal of Drying Technology*, 27(10), 1123-1131.

[6] AOAC., 2000. Official Methods of Analysis. 17th ed. Gaithersberg, MD, USA: Association of Analytical Communities.

[7] Re, R., Pellegrini, N., Proteggente, A., Pannala, A., Yang, M and Rice-Evans, C., 1999. Antioxidant activity applying an improved ABTS radical cation decolorization assay. *Journal of Free Radical Biology and Medicine*, 26, 1231-1237.

[8] Benzie, I.F. and Strain, J.J., 1996. The Ferric Reducing Ability of Plasma (FRAP) as a measure of ‘‘antioxidant power’’: The FRAP assay. *Journal of Analytical Biochemistry*, 239, 70-75.

[9] Kajsongkram, T., Rotamporn, S., Limbunruang, S. and Sirinan, T., 2015. Development and validation of a HPLC method for 6-gingerol and 6-shogaol in joint pain relief gel containing ginger (*Zingiber officinale*). *International Journal of Medicine and Health Science*, 9(12), 813-817.

[10] Mazaud, F., Rottger, A. and Steffel, K., 2002. *GINGER: Post-Production Management for Improved Market Access*. [online] Available at: https: // www. scribd. com/ document/ 209439414/Post-Harvest-Compendium-Ginger

[11] Jogi, B.S., Singh, I.P., Dua, H.S. and Sukhija, P.S., 1972. Changes in crude fibre, fat and protein content of ginger at different stages of ripening. *Indian Journal of Agricultural Science*, 42, 1011 - 1015.

[12] Nybe, E.V., Nair, P.C.S and Mohankumaran, N., 1982. Assessment of yield and quality components of ginger. In: Nair, M.K., Premkumar, T., Ravindran, P.N. and Sarma, Y.R., *Proceedings of National Semiliar on Ginger and Turmeric,* Kasaragod, India: Central Plantation Crops Research Institute.

[13] Ratnambal, M.J., Gopalam, A. and Nair, M.K., 1987. Quality evaluation in ginger (*Zingiber officinale* Rosc.) in relation to maturity. *Journal of Plant and Crops*, 15, 108-117.

[14] Chumroenphat, T., Khanprom, I. and Butkhup, L., 2011. Stability of phytochemicals and antioxidant properties in ginger with different drying methods. *Journal of Herbs, Spices and Medicinal Plants*, 17(4), 361-374.

[15] Harish, R. and Shivanandappa, T., 2006. Antioxidant activity and hepatoprotective potential of *Phyllanthus niruri*. *Journal of Food Chemistry*, 97, 122-129.

[16] Hassimotto, N., Genovese, M. and Lajolo, F., 2005. Antioxidant activity of dietary fruit, vegetables, and commercial frozen fruit pulps. *Journal of Agricultural Food Chemistry*, 53(8), 2928-1935.

[17] Chen, I., Chang, C., Wang, C., Shyu, Y. and Chang, T., 2008. Antioxidant and antimicrobial activity of Zingiberaceae plants in Taiwan. *Journal of Plant Food Human Nutrition*, 63(1), 15-20.

[18] Teferra, T., Kifle, A., Tefera, A., Abate, S., Sima, B., Astatike, A., Habte, T and Samuel, A., 2015. *Ginger (Zingiber Oficinale Rosec.): Production, Postharvest Handling, Processing and Marketing - A Comprehensive Extension Package Manual.* [online] Available at: https://www.researchgate.net/publication/279442041_Ginger_Zingiber_Oficinale_Rosec_Production_Postharvest_Handling_Processing_and_Marketing_-_A_Comprehensive_Extension_Package_Manual

[19] Lawrence, B.M., 2000. Progress in essential oils. Ginger oil. *Perfumer and Flavorist*, 25(2), 55-58.

[20] Connel, D.W. and Jordan, R.A., 1971. Composition and distinctive volatile flavor characteristics of the essential oil from Australian-grown ginger (*Zingiber officinale*). *Journal of the Science of Food and Agriculture*, 22, 93-95.

[21] Weiss, E.A. 1997. *Essential Oil Crops*. Oxon: CAB International Publishing.

[22] Kiran, C.R., Chakka, A.K., Amma, K.P.P., Menon, A.N., Kumar, M.M.S. and Venugopalan., V.V., 2013. Essential oil composition of fresh ginger cultivars from North-East India. *Journal of Essential Oil Research,* 25(5), 380-387.

[23] Baranowski, J.D., 1986. Changes in solids, oleoresin, and (6)-gingerol content of ginger during growth in Hawaii. *Journal of Horticulture Science*, 21(1), 14-146.

[24] Weiss, E.A., 2002. *Spice Crops*. Oxon: CAB International Publishing.

[25] Bhatt, N., Waly, M., Musthafa, M.E. and Ali, A., 2013. *Ginger: A Functional Herb*. New York: Nova Science Publishers.

[26] Purseglove, J.N., Brown, E.G., Green, C.L. and Robbins, S.R.J., 1981. *Spices*. London: Longman.

[27] Wohlmuth, H., Leach, D.N., Smith, M.K. and Myers, S.P., 2005. Gingerol content of diploid and tetraploid clones of ginger (*Zingiber officinale* Roscoe). *Journal of Agriculture and Food Chemistry*, 53(14), 5772-5778.

[28] Yussef, K.M. and Mokhtar, S.M., 2014. Effect of drying methods on the antioxidant capacity, color and phytochemicals of *Portulaca oleracea* L. Leaves. *Journal of Nutrition and Food Sciences*, 4(6), 1-6.

[29] National Bureau of Agricultural Commodity and Food Standards., 2015. *Good agricultural practices for ginger*. [online] Available at: http: / / www.acfs.go.th/standard/download/eng/GAP-GINGER-ENG.pdf

[30] Reis, R.C., Castro, V.C., Devilla, I.A., Oliveira, C.A., Barbosa, L.S. and Rodovalho, R., 2013. Effect of drying temperature on the nutritional and antioxidant qualities of cumari peppers from Pará (*Capsicum chinense Jacqui*). *Brazilian Journal of Chemical Engineering*, 30(2), 337-343.

[31] Nwinuka, N.M., Ibeh, G.O. and Ekeke, G.I., 2005. Proximate composition and levels of some toxicants in four commonly consumed spices. *Journal of Applied Science and Environmental Management*, 9(1), 150-155.

[32] Balladin, D.A., Chang-Yen, I., McGaw, D.R. and Headley, O., 1996. Solar drying of West Indian ginger (*Zingiber officinale* Roscoe) rhizome using a wire basket dryer. *Journal of Renewable Energy*, 7(4), 409-418.

[33] Phowong, C., Thuwapanichayanan, R. and Jaisut, D., 2012. Effect of drying temperatures on drying kinetics, total phenolic content, antioxidant activities and color of ginger. *Journal of Agricultural Science*, 43(3), 460-463.

[34] An, K., Zhao, D., Wu, J., Xu. Y. and Xiao, G., 2016. Comparison of different drying methods on Chinese ginger (*Zingiber offinale* Roscoe): Changes in volatiles, chemical profile, antioxidant properties, and microstructure. *Journal of Food Chemistry*, 197, 1292-1300.

[35] Ok, S. and Joeng, W., 2012. Optimization of extraction conditions for the 6-shogaol-rich extract from ginger (*Zingiber officinale* Roscoe). *Journal of Preventive Nutrition and Food Science*, 17(2), 166-171.

[36] Puengphian, C. and Sirichote, A., 2008. [6]-gingerol content and bioactive properties of ginger (*Zingiber officinale* Roscoe) extracts from supercritical CO_2 extraction. *Asian Journal of Food and Agro-Industry*, 1(01), 29-36.

[37] Lee, S., Khoo, C., Halstead, C.W., Huynh, T. and Bensoussan, A., 2007. Liquid chromatographic determination of 6-, 8-, 10-gingerol, and 6-shogaol in ginger (*Zingiber officinale*) as the raw herb and dried aqueous extract. *Journal of AOAC International*, 90(5), 1219-1226.

Oily Sludge Biodegradation by Bacterial Isolates from Khurais Oil Field in Saudi Arabia

Fahad A. Al-Dhabaan*

Department of Biology, Science and Humanities College, Shaqra University, Al-Quwayiyah, Saudi Arabia

Received: 12 November 2018, Revised: 22 January 2019, Accepted: 28 February 2019

Abstract

This investigation was carried out to detect oily sludge biodegradation activity of bacterial isolates from Khurais oil field, Saudi Arabia. The understanding of different biodegradation capability was cleared in the light of amplifying Alkane Hydroxylase gene (*alkB*). Based on morphological and biochemical studies and 16S rRNA marker, our bacterial isolates were identified as *Klebsiella pneumoniae*, *Pseudomonas stutzeri, Pseudomonas alcaligenes* and *Bacillus cereus*. Varied degradation percentage of saturated and aromatic fractions for four bacterial isolates were recorded. Only *Pseudomonas alcaligenes* and *Bacillus cereus* amplified Alkane Hydroxylase genes were found with different identity percentage. Significant different for Alkane Hydroxylase (*alkB*) amino acids 3D modeling was cleared. SDS-PAGE technique reflected distinguished fraction variation among four bacterial isolates. Additionally, Alkane Hydroxylase gene (*alkB*) with the specific fraction of 41 kDa was only expressed in *Bacillus cereus* and *Pseudomonas alcaligenes.*

Keywords: Khurais oil field, oil sludge biodegradation, 16S rRNA, Alkane Hydroxylase gene, *alkB*, SDS-PAGE technique, amino acids 3D modeling
DOI 10.14456/cast.2019.6

1. Introduction

Petroleum hydrocarbons consist of 50- 80% of crude oil with many components like alkanes, cycloalkanes and aromatic alkanes [1]. However, there have been serious problems worldwide due to environmental contamination with such petroleum hydrocarbons. The oxidation of N-alkanes by bacterial growth is considered as a very common phenomenon in soil and water [2]. United States Environmental Protection Agency (US EPA) has categorized oily sludge as a hazardous organic complex (3 and 4) producing from human activities such as oil extraction, improper treatments, storage and transportation. Interestingly, cytotoxicity, carcinogenicity and mutagenicity for many of

*Corresponding author: Tel.: 966504893691
E-mail: ai_gentics80@yahoo.com

the oil sludge components were detected [5]. It could represent direct environmental impact of oil sludge contamination as natural habitats' alteration on the chemical and physical level. Different components were fractional from oil sludge which included volatile organic carbons (VOCs) and semi-volatile organic carbons (SVOCs) which turned to be genotoxicity influence [6]. The direct influence of oily sludge was a cumulative effect on the central nervous system (CNS) leading to dizziness, tiredness loss of memory and headache, and the effect depends on the duration of exposure [7].

Bioremediation is a promising approach to oil sludge accumulation, as it employs microorganisms to degrade or remove different pollutants such as organic compounds [8], hydrocarbons and heavy metals [9]. Nature and the amount of the hydrocarbons are considered as the main factors for petroleum hydrocarbons biodegradation. Saturates, aromatics, asphaltenes and resins are the four main classes of petroleum hydrocarbons [10]. Microbial degradation is essential and the most effective mechanism by which petroleum hydrocarbon could be cleaned up from the environment [11,12].

Many microorganisms like bacteria, yeast and fungi can primarily degrade hydrocarbons. The efficiency of biodegradation ranged from 6% to 82% for soil fungi and 0.13% to 50% for soil bacteria has been reported [13, 14]. Based on findings that bacteria are the most active agent in petroleum degradation, several bacteria are even known to feed exclusively on hydrocarbons and 22 genera of bacteria and 31 genera of fungi were reported with petroleum degradation capability [15].

Bacterial genera, *Gordonia, Brevibacterium, Aeromicrobium, Dietzia, Burkholderia*, and *Mycobacterium* isolated from contaminated petroleum residual soil were nominated as potential organisms for hydrocarbon degradation [16]. Also, polyaromatic hydrocarbons were degradated by *Sphingomonas* sp. [17]. Alkane hydroxylases (AHs) are the key enzymes in aerobic degradation of alkanes in petroleum-contaminated environments by catabolizing bacterial β-oxidation pathway which oxidized hydroxylate alkanes to alcohols, and fatty acids. Furthermore, numbers of bacteria have multiple Alkane hydroxylases with expanding potential of n-alkane range of the host strain via co-existence CYP153 like in *Dietzia* sp. [18].

Our investigation aimed to isolate bacteria from Khurais oil field for biodegradable ability of oil sludge by amplifying of Alkane Hydroxylase Gene (*alkB*) and diversity was performed via sequencing method. Amino acid sequencing modeling was performed to test Alkane Hydroxylase Gene (*alkB*) activity among bacterial isolates.

2. Materials and Methods

2.1 Sample collection

Oily sludge sample collected from Khurais oil field in Saudi Arabia in the boundary area of 2890 km (2,250 km southwest of Dhahran and 150 km east-northeast of Riyadh, 25.0715N, 48.0556E) in 2018. After 16 weeks of composting, samples were immediately collected from the composting containers in sterile plastic and transported to the laboratory. Samples were stored at 4 °C until further use.

2.2 Bacterial isolation

Enrichment technique applied for bacterial isolation was done by adding1% of oily sludge to 50 ml of sterile MM1 mineral medium as a sole carbon source [19]. Sample flasks were kept at 100 rpm and 30 °C. At every 5 days, 1 ml of sample was transferred to a fresh MM1 medium and incubated

under the same conditions. Surface spreading and streak plate techniques were applied on nutrient agar plates after 5 transferences.

2.3 Bacterial inoculums

After 24 h, 50 ml of bacterial inoculum (incubation at 30 °C, 100 rpm in a rotary shaker) were centrifuged at 9000 rpm for 15 min and bacterial cells were washed three times in the sterile MM1 mineral medium. Bacterial pellets were resuspended in MM1 mineral medium and kept in the rotary incubator for 24 h at 100 rpm and 30 °C to allow sufficent growth of bacteria.

2.4 Biodegradation of oily sludge in a liquid medium

Evaluation of oily sludge biodegradation capacity was performed through the Bartha respirometric method which was prescribed in technical standard L6.350 by CETESB and in NBR 14283/99. The experiments were carried out using 125 ml flasks. Bacterial isolates at 105-106 cells/ml in MM1 medium containing 1% of oily sludge as the sole carbon source were cultured for 40 days at 30 °C on shaking rotary at 100 rpm. Mineral medium and oily sludge without microbial inoculation were used as control sample [20].

2.5 Biodegradation assays

Liquid-liquid extraction was applied after the incubation period of 40 day to remove the remaining oily sludge in the liquid medium by the modification method from Bowman *et al.* [21]. Gas Chromatography model TRACE™ 1300 (Thermo Fisher,14800301) was used for fractions analysis. Internal standardization was applied to perform quantitative analysis by adding a known concentration of n-alkane C20 deuterated standard to the saturated fraction, and known concentrations of naphthalene, phenanthrene and chrysene reiterated standards to the aromatic fraction.

2.6 Bacterial 16S rRNA gene identification

In this investigation, 16S rRNA gene was applied as a molecular marker for bacterial identification. Total genomic DNA was extracted from our bacterial isolates through E.Z.N.A.® Bacterial DNA Kit (Omega Bio-TEK, D3350-01) according to manufacturer's protocol. A 16S rRNA region was amplified by PCR using 0.5 mM of forward primer, 27F (5′-AGA GTT TGA TCC TGG CTC AG-3′) and reverse primer 1492R (5′-CGG CTA CCT TGT TAC GAC TT-3′), 200 mM of each dNTP, 10 mM KCl PCR buffer, 2 mM $MgCl_2$ and 1.0 U Taq polymerase (Thermo Scientific, 500 U, #EP0402). Universal Gradient (peqSTAR 96) (Peqlab, Germany) was applied to perform amplification under following conditions: one cycle at 98 °C for 10 s, followed by 34 cycles at 98 °C for 1 s, 53 °C for 1 min and 72 °C for 15 s. A final extension step at 72 °C for 1 min was performed for 1 cycle. The reaction was held at 4 °C until the amplicons were removed from the thermal cycler. Agarose gel electrophoresis (1.5%) was applied for detecting PCR products with DigiDoc-it (Gel documentation analysis, UVP, England). Then, E.Z.N.A.® Gel Extraction Kit (Omega Bio-TEK, D2500-01) was used for purification. Purified fragments by Macrogen (Seoul, South Korea), purification and sequencing using an ABI3730 XL automatic DNA sequence were done. Amplified samples were identified by 16S rRNA nucleotide sequences using the Basic Local Alignment Search Tool (BLAST) program of the National Centre for Biotechnology Information (NCBI) for the closest species. Then, phylogenetic tree was constructed via Clustal Omega, Multiple Sequence Alignment (https://www.ebi.ac.uk/Tools/msa/clustalo/). Finally, ExPASy (Expert Protein Analysis

System) proteomics server of the Swiss Institute of Bioinformatics (http://us.expasy.org/ tools/ dna. html) was used to translate identified nucleotide sequences into protein sequences. The Simpsons Index of Diversity [22] was used to define the community structure.

2.7 PCR amplification of *alkB* genes

0.5 mM of forward primer *alkB*-1f 5AAYACNGCNCAYGARCTNGGNCAYAA3) and reverse primer *alkB*-1r (5-GCRTGRTGRTCNGARTGNCGYTG-3) was added to DreamTaq Green PCR Master Mix (2X) (Thermo Fisher Scientific, K1081) according to protocol to amplify partial alkB genes [23]. Thermal cycler conditions were performed as follows: 95 °C for 15 min, an initial enzyme activation step for 39 cycles of 94 °C for 1 min, annealing at 55 °C for 1 min, and extension at 72 °C for 1 min, 72 °C for 10 min as a last extension step.

2.8 Phylogenetic analysis of *alkB* genes

Alkane Hydroxylase gene (*alkB*) nucleotide sequences were identified using NCBI (https://www.ncbi.nlm.nih.gov/) database. The phylogenetic tree was then constructed using Clustal Omega, Multiple Sequence Alignment (https://www.ebi.ac.uk/Tools/msa/clustalo/).

2.9 Polyacrylamide Gel Electrophoresis (SDS-PAGE)

Total soluble proteins for bacterial isolates were purified through the Trifast solution (Trifast, VWR) according to manufacturer's protocol. For *alkB* single protein fraction purification, bounded protein was washed and dialyzed through 30 kDa MWCO Amicon Ultra dialysis spin column at 48 ºC. To identify fractions containing *alkB* protein product, 15% SDS-PAGE electrophoresis was applied. Selected fractions detected to contain *alkB* were concentrated, dialyzed with a 30 kDa MWCOAmicon Ultra dialysis spin column. Final concentrate of *alkB* single protein band was analyzed via 12%Tris–Tricine SDS-PAGE [24].

3. Results and Discussion

3.1 Bacterial identification

Bacteria cultured in the liquid mineral medium based on using oily sludge as the sole carbon source were isolated. Table 1 illustrates morphological and biochemical features for our bacterial isolates. Figure 1 showed amplified 16S rRNA gene products for bacterial isolates, based on the partial sequence of the 16S rRNA gene which applied as a molecular identification method. Four bacterial isolates (no. 1, 2, 3 and 4) were identified as *Klebsiella pneumoniae, Pseudomonas stutzeri*, *Pseudomonas alcaligenes* and *Bacillus cereus*, respectively. Table 2 showed the identification of oily sludge biodegradable bacteria with identity (%). Figure 2 showed constructed phylogenetic tree of four bacterial isolates under study comparing with highest identity isolates based on 16S rRNA gene sequences. *Pseudomonas stutzeri* was identified as the closest bacterial species to second biodegradation isolate which has 100% of identity when compared with the database.

Many studies used 16S rRNA genes as a molecular characterisation for crude oil sludge degrading bacteria [17]. Our identified bacterial isolates with oil sludge degradation ability were comparable to the findings of many studies. More light for employed 16S rRNA genes as a molecular characterisation tool was added to our findings via different identified genera, including

Stenotrophmonas, Pseudomonas, Bordetella, Brucella, Bacillus, Achromobacter, Ochrobactrum, Advenella, Mycobacterium, Mesorhizobium, Klebsiella, Pusillimonas and *Raoultella* with varied degrading polycyclic aromatic hydrocarbons (PAHs) ration according to partial 16S rRNA gene sequences [18]. Furthermore, our findings of bacterial confirmatory identification for polycyclic aromatic hydrocarbons biodegradation were in accordance with confirmed *Pantoea agglomerans, Acinetobacter lwoffii* and *Bacillus thuringiensis* through partial 16S rRNA gene sequencing molecular analysis [25].

After 40 days of oily sludge incubation, oily sludge degradation was evaluated for bacterial isolates. Figure 3 showed saturated and aromatic fractions degradation percentage. *Pseudomonas stutzeri* reflected the highest saturated fraction degradation (89.7% ± 0. 7). On the contrary, *Pseudomonas alcaligenes* showed the highest aromatic fraction degradation (61.8%± 2.3). *Klebsiella pneumoniae, Pseudomonas alcaligenes* and *Bacillus cereus* were arranged discerningly for saturated oil degradation. Aromatic oil degradation was arranged ascending for *Klebsiella pneumoniae, Bacillus cereus, Pseudomonas stutzeri* and *Pseudomonas alcaligenes*. According to our bacterial isolates with

Table 1. Morphological and biochemical features of oily sludge bacteria.

Morphological and biochemical features	**Bacterial isolates**			
	First	Second	Third	Fourth
Morphological features				
Grams staining	-	-	+	+
Morphology	Rods	Rods	Rods	Rods
Biochemical features				
Oxidase	-	+	+	-
Catalase	+	+	+	+
Indole production	-	-	-	-
Citric utilization	+	+	+	+
Gelatin hydrolysis	-	+	+	-
Urease	+	-	-	-
Starch hydrolysis	+	+	-	+
Nitrate reduction	+	+	+	-
Mannitol	+	+	-	-
Casein hydrolysis	-	-	-	+
Methyl red test	-	-	-	-

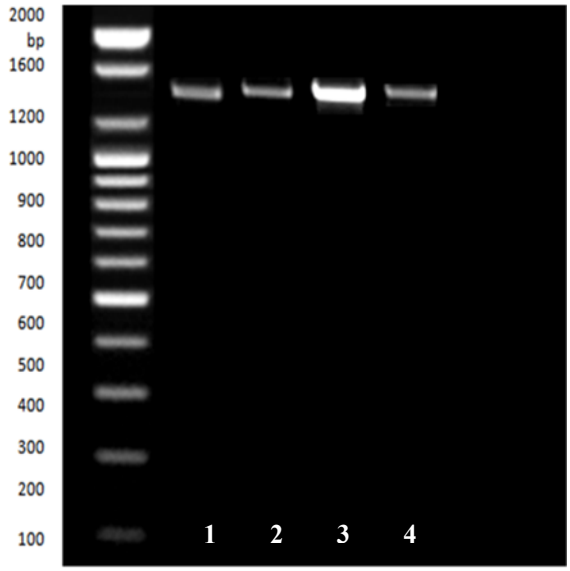

Figure 1. Amplified products for 16S rRNA molecular marker gene.
1. Klebsiella pneumoniae 2. Pseudomonas stutzeri
3. Pseudomonas alcaligenes 4. Bacillus cereus

Table 2. Molecular identification of 16S rRNA gene partial sequence for oily sludge bacteria.

Isolate	Identification	Identity (#)
No.1	*Klebsiella pneumoniae*	99
No. 2	*Pseudomonas stutzeri*	100
No. 3	*Pseudomonas alcaligenes*	99
No.4	*Bacillus cereus*	99

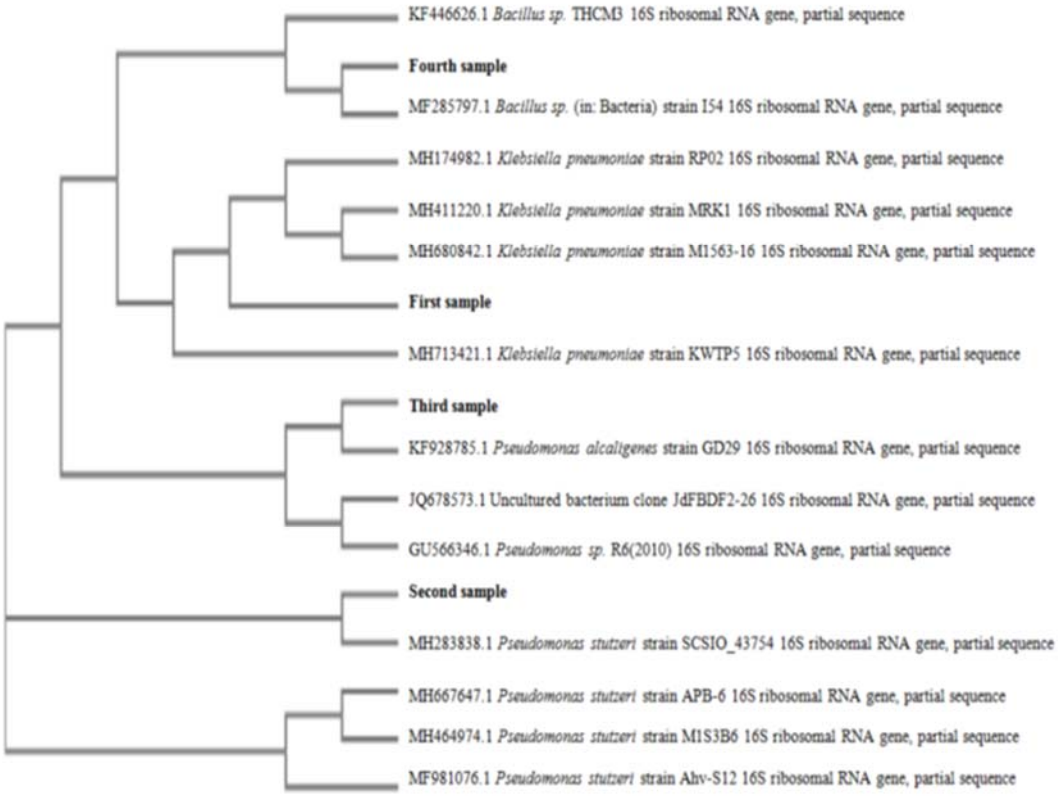

Figure 2. Phylogenetic tree for four bacterial isolates based on 16S rRNA gene sequences.

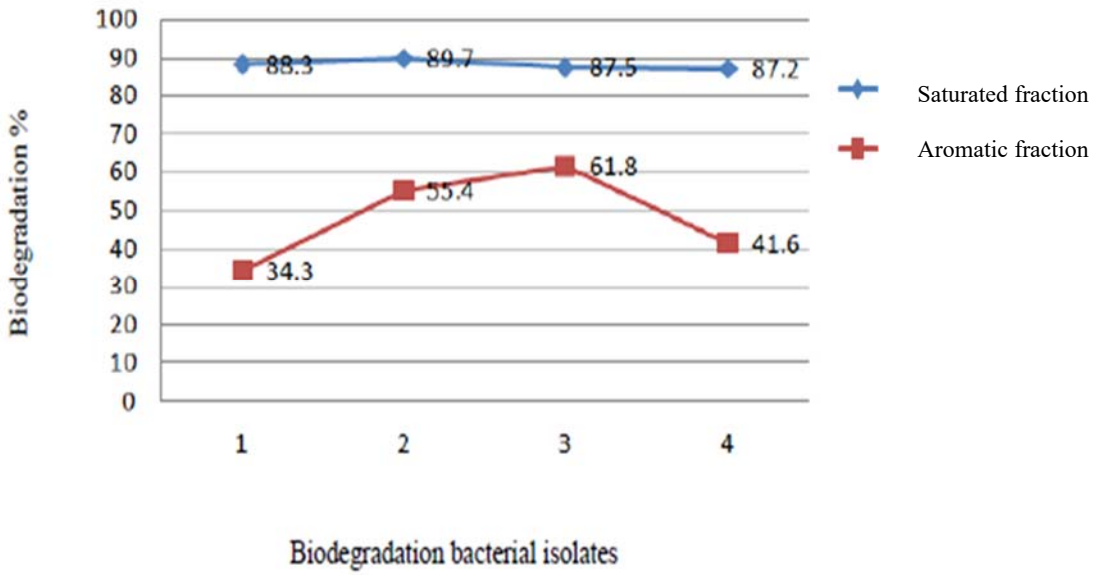

Figure 3. Biodegradation for four bacterial isolates.
1. Klebsiella pneumoniae 2. Pseudomonas stutzeri
3. Pseudomonas alcaligenes 4. Bacillus cereus

oil sludge degradation capability, *Pseudomonas stutzeri* strain AOR1 with 90% efficiency and *Klebsiella pneumoniae* strain AOR2 with 70% efficiency in oil recovery from oil sludge were recorded [26, 27]. Additionally, unique oily sludge degradable capability for *Bacillus cereus* was previously detected [28]. Our findings could be cleared in the light of released bio-surfactant by *Bacillus subtilis* 3KP which contacted with the hydrocarbons [29]. In accordance with our findings on evaluating hydrocarbons biodegrading capability, *Pseudomonas stutzeri* AOR1 and *Klebsiella pneumoniae* AOR2 which were identified by 16S rRNA sequencing reflected different degradation of long chain hydrocarbons from produced oil sludge in Abadan refinery, Iran [30].

Amplifying of *alkB*, diversity of *alkB* was amplified for four biodegradable bacterial isolates through specific molecular marker primer. As shown by Figure 4, only *Pseudomonas alcaligenes* and *Bacillus cereus* amplified *alkB*. In contrast, *Klebsiella pneumoniae* and *Pseudomonas stutzeri* did not amplify *alkB*. Optimized different *alkB* primers were in accordance with a combination of three *alkB* -targeting primers used to enhance the detection of the *alkB* gene in previously isolated alkane-degrading bacteria [31]. Using this approach, *alkB* -related PCR products were detected in 79% of the strains tested. Significant identity percentage of our *alkB* sequences was in accordance with constructed cluster analysis of *alkB* sequences from different biodegradable microorganisms and reflected very little sequence identity from known organisms (only 71 % with *Burkholderia cepacia*) and other unknown uncultured bacteria (79 % identity with uncultured bacterium DQ288068) [32].

Purified (*alkB*) sequences identification showed that *Pseudomonas alcaligenes* reflected 100% of identity for *alkB*. On the contrary, *Bacillus cereus* reflected the lowest identity (74%) for *alkB* (Figures 5 and 6, Table 3). More evidence was added to our findings for *alkB* diversity based on varied distributions of *alkB* between bacterial genomes and based on potentially important roles of unknown or less common alkane degrades in nature [33]. More support for *alkB* sequence

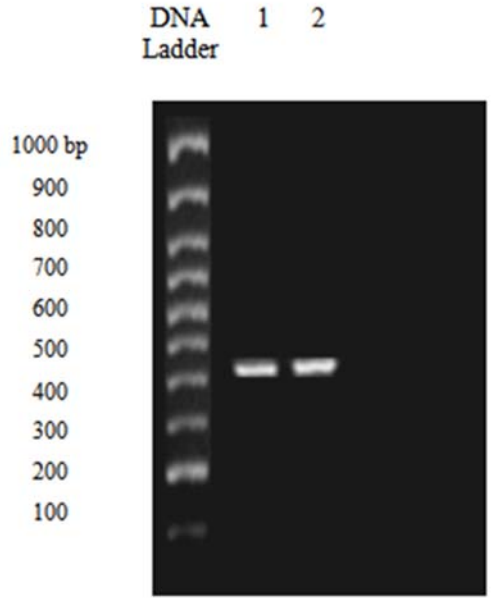

Figure 4. Amplified products for Alkane Hydroxylase gene (*alkB*).
1. *Pseudomonas alcaligenes*
2. *Bacillus cereus*

(A) (B)

```
>Pseudomonas alcaligenes partial alkB gene,
     AGTTGACATC ACCGCGACGT GGCCACCCCG GTGGACCCGG CCTCCTCGCG CATGGGTGAA        60
     CATATCTACC GCTTCCTCCT GCGCGAGATG CCAGGTGGTT ATCGCCGCGC CTGGCAGCTG       120
     GAGAAGGAAC GCCTGGCGCG CTGCAATAAA TCGGTCTGGA GTCTGGACAA CGAAGTGCTG       180
     CAACCGGCGC TGATCAGCCT GGCACTGTAT GGCGCACTGG TCGCCGTGTT CCCTTCTGGG       240
     GCGGCTTCCG GCCTGGCCCT GCTGCCCTAC CTGCTGCTCA CGGAAGCAGT GCGCC            295
//
```

(C)

Figure 5. Data analysis for Alkane Hydroxylase gene (*alkB*) for *Bacillus cereus* isolate.

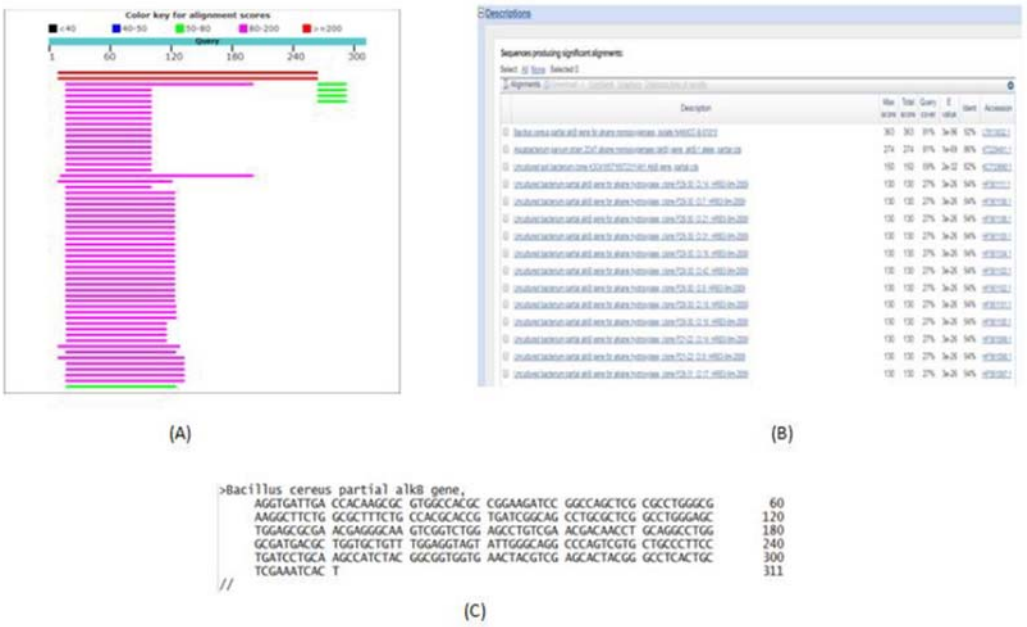

Figure 6. Data analysis for Alkane Hydroxylase gene (*alkB*) for *Pseudomonas alcaligenes* isolate.

Table 3. Molecular identification of Alkane Hydroxylase gene (alkB) for oily sludge bacteria.

Isolates	identification	Identity (%)
No. 3	*Pseudomonas alcaligenes*	100
No. 4	*Bacillus cereus*	92

diversity was found for marine Gammaproteobacteria which reflected identities sequence with an average of only 73% (with a range of 60% to 94% sequence identities). Also, *alkB* sequence diversity was lower in deep water samples comparing with shallow water samples (<100 m) on the continental shelf but not much different in response to levels of alkanes>26).

Fractionation of four bacterial isolates and total soluble proteins carried out via polyacrylamide gel electrophoresis (SDS- PAGE) technique reflected distinguished fraction variation. As shown in Figure 7, *Pseudomonas stutzeri* fractionated 10 protein fractions and *Klebsiella pneumoniae* expressed 12 fractions. Also, *Bacillus cereus* showed 7 fractions and 9 protein bands were shown by *Pseudomonas alcaligenes*. Based on protein patterns variation of four bacterial isolates under study, polymorphism (%) was evaluated. *Klebsiella pneumoniae* showed the highest genetic variation with 91.6% of polymorphism. Meanwhile, *Pseudomonas alcaligenes*

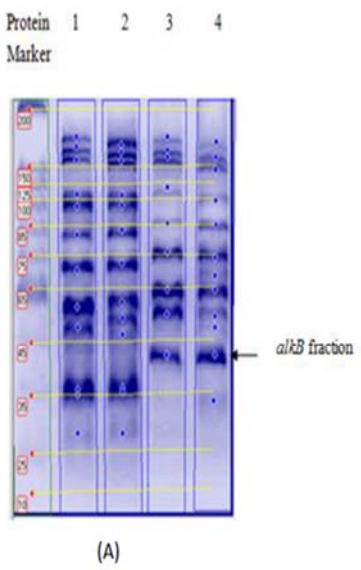

Fractions molecular weight (KDa)	*Pseudomonas stutzeri*	*Klebsiella pneumonia*	*Bacillus cereus*	*Pseudomonas alcaligenes*
	-	-	174	-
	171	-	-	-
	-	166	-	-
	-	160	-	-
	-	-	158	-
	-	154	-	-
	150	-	-	-
	-	-	-	144
	-	-	122	-
	117	-	-	-
	-	102	-	-
	98	-	-	-
	-	-	85	85
	-	83	-	-
	82	-	-	-
	-	-	78	-
	-	-	-	75
	-	74	-	-
	70	-	-	-
	-	-	-	69
	-	-	65	-
	-	-	-	64
	-	60	-	-
	56	-	-	-
	-	-	55	-
	-	-	-	54
	-	52	-	-
	50	-	-	50
	-	48	-	-
	-	-	**41**	**41**
	36	-	-	-
	-	35	-	-
	-	34	-	-
	-	-	-	33
	30	30	-	-

Figure 7. Protein fingerprinting patterns of four biodegradable bacterial isolates.

Table 4. Total fractions, polymorphism of protein fractions for bacterial isolates.

Bacterial isolates	**Total fractions**	**Polymorphic fractions**	**Common fractions**	**Polymorphism %**
Pseudomonas stutzeri	10	8	2	80.0
Klebsiella pneumoniae	12	11	1	91.6
Bacillus cereus	7	6	1	85.7
Pseudomonas alcaligenes	9	6	3	66.6

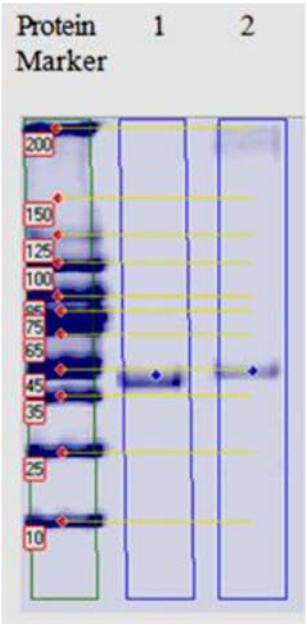

Figure 8. Alkane Hydroxylase (*alkB)* purified specific band for two bacterial isolates.
1. Pseudomonas alcaligenes
2. Bacillus cereus

reflected lowest genetic dissimilarity with 66.6% of polymorphism (Table 4). Interestingly, only *Bacillus cereus* and *Pseudomonas alcaligenes* expressed remarkable *alkB* with 41 kDa which is indicated by advanced protein purification technique (Figure 8). In accordance with detection of *alkB* product with unique molecular weight, polyacrylamide gel electrophoresis (SDS-PAGE) technique was applied to detect alkane hydroxylase-1 from *Alcanivorax borkumensis* in *Escherichia coli* [34]. Furthermore, purified *alkB* was monitored and detected with 41 kDa through SDS-PAGE technique [35]. More light was added to our findings for screening biodegradation activity by employing SDS-PAGE for detecting biodegradable plastic-degrading enzyme (PaE) from *Pseudozyma antarctica* JCM 10317 [36].

4. Conclusions

The results of this study indicate the efficiency of oily sludge biodegradation activity for bacterial isolates from Khurais oil field, Saudi Arabia which were identified through morphological, biochemical and 16S rRNA molecular marker as *Klebsiella pneumoniae, Pseudomonas stutzeri, Pseudomonas alcaligenes* and *Bacillus cereus*. In addition, different degradation percentage of oily sludge was evaluated for four bacterial isolates. Furthermore, Alkane Hydroxylase gene (*alkB*) was amplified, sequenced and identified. Remarkable Alkane Hydroxylase (*alkB*) sequences were recorded among *Klebsiella pneumoniae, Pseudomonas stutzeri, Pseudomonas alcaligenes* and *Bacillus cereus*. Finally, Alkane Hydroxylase gene (*alkB*) with the specific fraction of 41 kDa was only expressed in *Bacillus cereus* and *Pseudomonas alcaligenes*.

References

[1] Bojes, H.K. and Pope, P.G. 2007. Characterization of EPA's 16 priority pollutant polycyclic aromatic hydrocarbons (PAHs) in tank bottom solids and associated contaminated soils at oil exploration and production sites in Texas. *Regulatory Toxicology and Pharmacology*, 47(3), 288-295.

[2] Mishra, S., Jyoti, J., Kuhad, R.C. and Lai, B. 2001. In situ bioremediation potential of an oil sludge-degrading bacterial consortium. *Current Microbiology*, 43, 328-335.

[3] Wang, W., Zhong, R. and Shan, D. 2014. Indigenous oil-degrading bacteria in crude oil-contaminated seawater of the Yellow Sea, China. *Applied Microbiology and Biotechnology*, 98, 7253-7269.

[4] Cao, J., Lai, Q. and Yuan, J. 2015. Genomic and metabolic analysis of fluoranthene degradation pathway in *Celeribacter indicus* $P73^T$. *Scientific Report*, 13(5), 7741-7753.

[5] Alisi, C., Musella, R. and Tasso, F. 2009. Bioremediation of diesel oil in a co-contaminated soil by bioaugmentation with a microbial formula tailored with native strains selected for heavy metals resistance. *Science of the Total Environment*, 407, 3024-3032.

[6] Plociniczak, T., Kukla, M. and Wątroba, R. 2013. The effect of soil bioaugmentation with strains of *Pseudomonas* on Cd, Zn and Cu uptake by *Sinapis alba* L. *Chemosphere*, 91, 1332-1337.

[7] Calvo, C., Toledo, F.L. and Gonzalez-Lopez, J. 2006. Surfactant activity of a naphthalene degrading *Bacillus pumilus* strain isolated from oil sludge. *Journal of Biotechnology*, 109 (3), 255-262.

[8] Bartha, R. and Pramer, D. 1965. Features of flask and method for measurement of the persistence and biological effects of pesticides in soil. *Soil Science*, 100(1), 68-70.

[9] Camargo, H., Nusspaumer, G., Abia, D., Briceno, V., Remacha, M. and Ballesta, J.P. 2011. The amino terminal end determines the stability and assembling capacity of eukaryotic ribosomal stalk proteins P1 and P2. *Nucleic Acids Research,* 39(9), 3735-43.

[10] Simpson, E.H. 1949. Measurement of diversity. *Nature*, 163, 688.

[11] Colwell, R.R., Walker, J.D. and Cooney, J.J. 1977. Ecological aspects of microbial degradation of petroleum in the marine environment. *Critical Reviews in Microbiology*, 5 (4), 423-445.

[12] Atlas, R.M. 1992. Petroleum microbiology. In J. Lederberg *et al.*, eds. *Encyclopedia of Microbiology*, pp. 363-369, Baltimore, USA: Academic Press.

[13] Lal, B. and Khanna, S. 1996. Degradation of crude oil by *Acinetobacter calcoaceticus* and *Alcaligenes odorans*. *Journal of Applied Bacteriology*, 81 (4), 355-362.

[14] Jones, J., Knight, M. and Byron, J.A. 1970. Effect of gross population by kerosene hydrocarbons on the microflora of a moorland soil. *Nature*, 227, 1166.

[15] Pinholt, Y., Struwe, S. and Kjoller, A. 1979. Microbial changes during oil decomposition in soil. *Holarctic Ecology*, 2, 195-200.

[16] Bartha, R. and Bossert, I. 1984. The treatment and disposal of petroleum wastes. In R.M. Atlas, ed. *Petroleum Microbiology*, pp. 553-578, New York, USA: Macmillan.

[17] Chaillan, F., Le Fleche, A. and Bury, E. 2004. Identification and biodegradation potential of tropical aerobic hydrocarbon degrading microorganisms. *Research in Microbiology*, 155 (7), 587-595.

[18] Daugulis, A. J. and McCracken, C. M. 2003. Microbial degradation of high and low molecular weight polyaromatic hydrocarbons in a two-phase partitioning bioreactor by two strains of *Sphingomonas* sp. *Biotechnology Letters*, 25 (17), 1441-1444.

[19] Obi, L., Atagana, H. and Adeleke, R. 2016. Isolation and characterisation of crude oil sludge degrading bacteria. *Springer Plus*, 5, 1946.

[20] Bahobail, A., Gad El-Rab, S.M.F. and Amin, G.A. 2016. Locally isolated bacterial strains with multiple degradation potential capabilities on petroleum hydrocarbon pollutants. *Advances in Microbiology*, 6, 852-866.
[21] Bowman, V.C., Francis, J.E., Riding, J.B., Hunter, S.J. and Haywood, A.M. 2012. A latest Cretaceous to earliest Paleogene dinoflagellate cyst zonation from Antarctica, and implications for phytoprovincialism in the high southern latitudes. *Review of Palaeobotany and Palynology*, 171, 40-56.
[22] Das, R. and Kazy, S.K. 2014. Microbial diversity, community composition and metabolic potential in hydrocarbon contaminated oily sludge: prospects for in situ bioremediation. *Environmental Science and Pollution Research*, 21(12), 7369-89.
[23] Hara, E., Kurihara, M., Nomura, N., Nakajima, T. and Uchiyama, H. 2013. Bioremediation field trial of oil-contaminated soil with foodwaste compost. *JJSCE*, 1(1), 125-132.
[24] Afifi1, A., Motamedi, H., Alizadeh, B. and Leilavi. B. 2015. Isolation and identification of oil degrading bacteria from oil sludge in Abadan oil refinery. *Environmental and Experimental Biology*, 13, 13-18.
[25] Mishra, S., Singh, S.N. and Pande, V. 2014. Bacteria induced degradation of fluoranthene in minimal salt medium mediated by catabolic enzymes in vitro condition. *Bioresource Technology*, 164, 299-308.
[26] Wasmund, K., Kathryn, A., Burns, D., Kurtb, I. and Bourne D. G. 2009. Novel alkane hydroxylase gene (alkB) diversity in sediments associated with hydrocarbon seeps in the Timor Sea, Australia. *Applied and Environmental Microbiogy*, 75 (23), 7391-7398.
[27] Obi, E., Akunyili, D.N., Ekpo, B. and Orisakwe, O.E. 2006. Heavy metal hazards of Nigerian herbal remedies. *Science of the Total Environment*, 369(1-3), 35-41.
[28] Kitamoto, H.K., Shinozaki1, Y., Cao, X., Morita, T., Konishi, M., Tago, K., Kajiwara , H., Koitabashi, M., Yoshida, S., Watanabe, T., Sameshima-Yamashita, Y., Nakajima-Kambe, T. and Tsushima, S. 2011. Phyllosphere yeasts rapidly break down biodegradable plastics. Kitamoto et al. *AMB Express* 2011, Nov. 29, 1:44. Doi: 10.1186/2191-0855-1-44.
[29] Cerqueira, V.S., Hollenbach, E.B., Maboni, F., Vainstein, M.H., Camargo, F.A., do Carmo, R. Peralba M. and Bento, FM. 2011. Biodegradation potential of oily sludge by pure and mixed bacterial cultures. *Bioresource Technology*, 102(23), 11003-10.
[30] Ni'matuzahroh, N. Trikurniadewi, A.R.A. Pramadita, I. A. Salamun, P. F. and Sumarsih, S. 2017. Biodegradation of naphthalene and phenanthren by *Bacillus subtilis* 3KP. *AIP Conference Proceedings,* 1854, 020026. doi: 10.1063/1.4985417.
[31] Xu, N.N., Bao, M.T., Sun, P.Y. and Li, Y. M. 2013. Study on bioadsorption and biodegradation of petroleum hydrocarbons by a microbial consortium. *Bioresource Technology,* 149, 22-30.
[32] Vomberg, A. and Klinner, U. 2000. Distribution of alkB genes within n-alkane-degrading bacteria. *Journal of Applied Microbiology*, 89(2), 339-48.
[33] Nie, Y., Chi, C.-Q., Fang, H., Liang, J.-L., Lu, S.-L., Lai, G.-L., Tang, Y.-Q. and Wu, X.-L. 2014. Diverse alkane hydroxylase genes in microorganisms and environments. *Scientific Reports*, 4, 4968.
[34] Wong, K., Quilty, B. and Surif, S. 2013. Degradation of crude oil in the presence of lead (Pb) and cadmium (Cd) by a metal adapted consortium culture. *Advances in Environmental Biology*, 7(4), 577-585.
[35] Eidani, S.Z., Shahraki, M.K., Gasemisakha, F., Hahsemi, M. and Bambai, B. 2012. Cloning and expression of alkane hydroxylase-1 from *Alcanivorax borkumensis* in *Escherichia coli*. *Toxicology and Industrial Health*, 28(6), 560-5.
[36] Hazaimeh, M., Abd Mutalib, S., Abdullah, P.S., Kok Kee, W. And Surif, S. 2014. Enhanced crude oil hydrocarbon degradation by self- immobilized bacterial consortium culture on sawdust and oil palm empty fruit bunch. *Annals of Microbiology*, 64(4), 1769-1777.

Assessing the Impact of Urban Encroachment on Agricultural Land in Kafr El-sheikh Governorate using GIS and Remotely Sensed Data

Mariam Zaky Mohamed* and Dalia M. M. Yacout

Institute of Graduate Studies and Research, Alexandria University, Alexandria, Egypt

Received: 2 September 2018, Revised: 24 January 2019, Accepted: 5 March 2019

Abstract

Urban encroachment is one of the top challenges facing developing countries due to the expansion of unplanned constructions. It is associated with increment in basic services including water, electricity and sewage. Nowadays in Egypt, lack of monitoring and governmental control on new constructions causes environmental problems, threatens the current infrastructure and may lead to problems in food security. Remote sensing and GIS are effective tools to map and analyse urban encroachment using Landsat images which provide needed data for measuring the change in urban area during the period of study. The aim of this study is to estimate the changes in agricultural area due to urban encroachment in Kafr El-sheikh Governorate, Egypt by using remotely sensed Landsat multispectral images for the period between the years 2010 to 2016. Software (ERDAS IMAGINE 2014 and ArcGIS 10.3) has been used for processing and analysing remote sensing data. Results concerning the agriculture land revealed that two main issues were developed during this period. First, a loss of 77.2 km² (about 3.1% of total fertilized land in Kafr El-sheikh Governorate) is due to urban encroachment from illegal construction of settlements and fish farms. Second, an increase of more than 20 km² is due to land reclamation in non-developing areas, around the northern part of Lake Burullus and eastern part of the study area. Agriculture and fishing sectors, which present the first and largest economic sectors in the study area need to get more attention from the Government because these are most influenced and damaged sectors by urban encroachment. Our study recommends conducting further studies investigating the urban encroachment for the whole region using remote sensing data and GIS tool. Furthermore, in order to prevent the illegal constructions, the application of law in Egypt has to be enhanced and the essential services has to be provided for the increase in the development of rural areas.

Keywords: Land cover change, urban encroachment, remote sensing, GIS
DOI 10.14456/cast.2019.5

*Corresponding author: Tel.: +201282290170
E-mail: m.zaky@alexu.edu.eg

1. Introduction

The global population has grown dramatically during the last century. Meanwhile, we have witnessed an unprecedented concentration of population into urban places around the world. Urban sprawl became a global phenomenon in both developed and developing countries [1]. Urban encroachment is not just a manifestation of a population explosion and demographic change, or even of the vast impersonal forces of globalization, it is a result of failure of national and urban housing policies and laws delivery. People who live in unplanned settlements lack the essential services and face several problems such as environmental, planning, health and social problems [2].

Most urban sprawl studies focused on the relationship between urbanization and environmental change in developed countries but there is a need for efforts to treat these questions in developing countries. This study approached to understand the current and future trends of urban growth in Alexandria, Egypt by using remote sensing and GIS techniques. One of the most important findings in this study area is the loss of cultivated land in favor of urban expansion [3]. Many studies [4-6] used multi-temporal remotely sensed data to study the change in land cover and land use and its impacts on agriculture areas. These studies concluded that urban encroachment regularly occurs through the deduction of agriculture land.

The cultivated areas in the Nile Valley and Delta are suffering from a serious problem of urbanization. This problem has caused an irretrievable loss of very fertile suitable soils. The problem is characterized by a very severe status and rate while the risk is severe. Shalaby [7] used remotely sensed data (Aerial photographs) for assessing the environmental condition of the study site. Another study [8] presented the effects of urban encroachment onto previously cultivated lands "urbanization". The researcher found that the expansion of thousands of small villages around the agricultural lands represents a risk that leads to loss in the agricultural productivity and degradation of water quality. Change detection has to be studied in order to determine the change in land cover, understanding the relationship between the human and environment and to use this information in better environmental management.

The Egyptian Northern Lakes have been major areas of fish production in Egypt. The fishing sector in Egypt is affected by urban encroachment caused by the violation of water resources from building illegal fish farms around Lake Burullus and Rosetta branch. Another type of violation from urban encroachment is drying-up the borders of Lake and Rosetta Nile branch to expand land area that causes a decrease in the total area of Lake. In addition, illegal fish farms are classified as a pollutant source because of the nutrients and generated wastes from this activity which causes changes in the ecosystem [8].

Nowadays, urban encroachment is an ongoing problem that has to be faced in Egypt. It has an impact on our daily life. Kafr El-sheikh Governorate was taken as a study area to assess the urban encroachment impact on its agricultural land. The aim of the study is to measure the changes in agriculture land resulting from urban encroachment by using remotely sensed data and GIS tools.

2. Materials and Methods

Kafr El-sheikh Governorate, a part of the Nile Delta, is one of the oldest intensely cultivated areas in Egypt. The governorate has a total population of about 3.3 million inhabitants [9]. It includes a variety of environmental habitats: Burullus Bay, Lake Burullus, Nile branch and the adjacent agricultural, urban and coastal area. The study area is located in the northern part of the Nile Delta, extends from 30° 59′38″ to 31° 36 ′00″ Latitude and from 30° 21′40″ to 31° 18′40″ Longitude. The governorate bordered from north by the Mediterranean Sea, with about 100 km of coastline, from

the south by Gharbeya Governorate, from the east by Dakahleya Governorate and from the west by Rosetta city where the Rosetta branch of the River Nile flows into the sea (Figure 1.).

Kafr El-sheik Governorate covers a total area of about 3754.121 km^2 including 10 districts, 11 cities, and 69 rural local units which consist of 143 villages, in addition to Manzala lake (about 600 km^2). According to the Central Agency for Public Mobilization and Statistics, 76.1% of the Kafr El-sheikh Population governorate lives in rural areas, which represents 81% of the total number of residential buildings. The rest of the population (23.9%) lives in urban areas, which presented 19% of the total number of residential buildings. That explains the sweep of the form of rural building in Kafr El- sheikh Governorate [9]. Most of the study area can be classified as cultivated land, which covered about 2310 km^2 (more than 66% of the total area). The area is famous for producing rice, beets, wheat and cotton. The nature of the area helps in maintaining three main activities: crop, animal and fish production [10]. Due to unplanned building extension new environmental burdens took place. Figure 2 presents onsite photos of water pollution in boundaries of Lake Burullus on 30 March 2018.

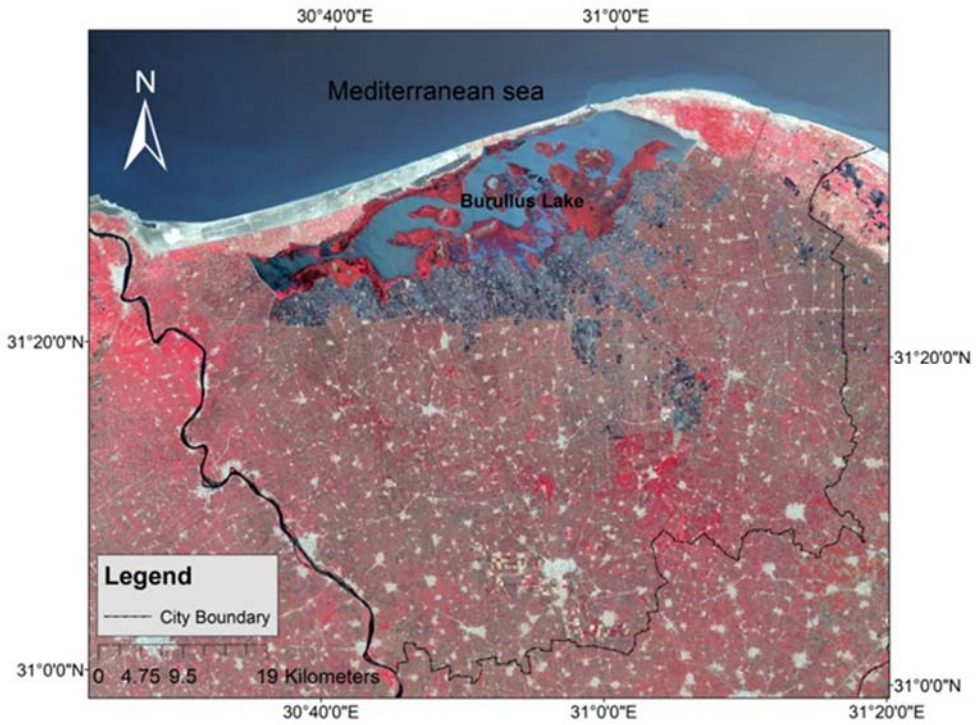

Figure 1. The location of study area

Figure 2. Violation of building around Lake Burullus

Loss of agriculture land from urban encroachment has been measured by available remote sensing data. Landsat 8 and Landsat 5 image (path 177, row 38, covering Kafr El-sheikh City) acquired on 19 Sep, 2016 and 18 Aug, 2010. These dates were the closest available data for the same agricultural season. Comparison between images dated in years 2010 to 2016 was chosen, as 2010 represents the status of the area before the political instability of the country in 2011 when most of illegal law violation of the lands happened. As for 2016 image, it was the most recent available image of the area clear with zero clouds.

Applied framework of methodology is presented in Figure 3. A polygon of Kafr El-sheikh Governorate boundary was used to clip the study area from the satellite images. This polygon was the last database updated of Central Agency for Public Mobilization and Statistics.

After clipping study area, Normalized Difference Vegetation Index (NDVI) was used for illustrating vegetation areas in both of images by using equation NDVI = (NIR - Red) / (NIR + Red). This index depends on visible and near-infrared bands of the electromagnetic spectrum for determining the density of green area on a patch of land [11]. The index produced an image with a highlight on vegetation area, which gained a positive pixel value and the other phenomenon gained pixel value less than or equal zero. By using conditional equation, vegetation areas have been extracted from NDVI index as it can be seen in Figure 4. Values of vegetation and non-vegetation areas have been recoded and giving numbers: 1 for vegetation and 0 for any other phenomenon. These steps were done for both images.

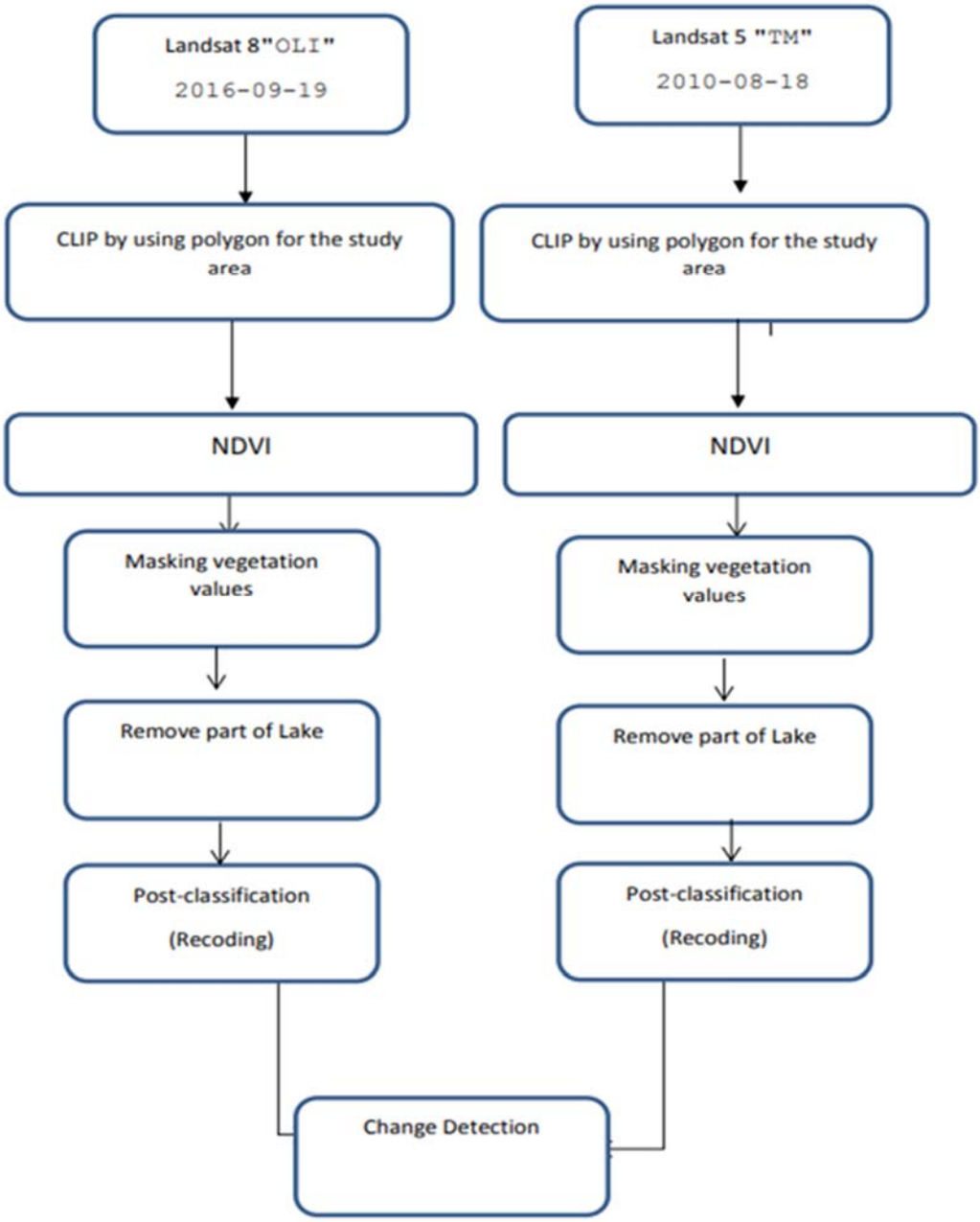

Figure 3. Framework of applied methodology

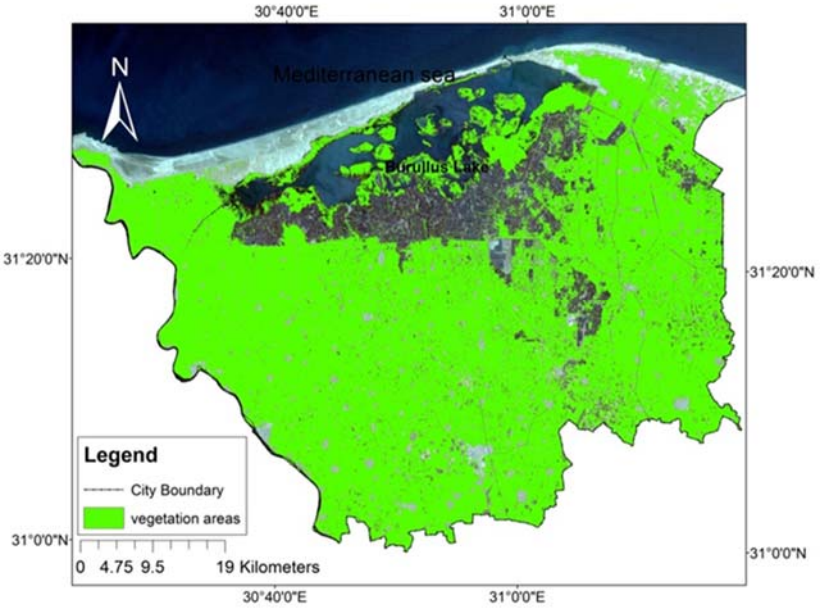

Figure 4. Extracting vegetation areas from NDVI index

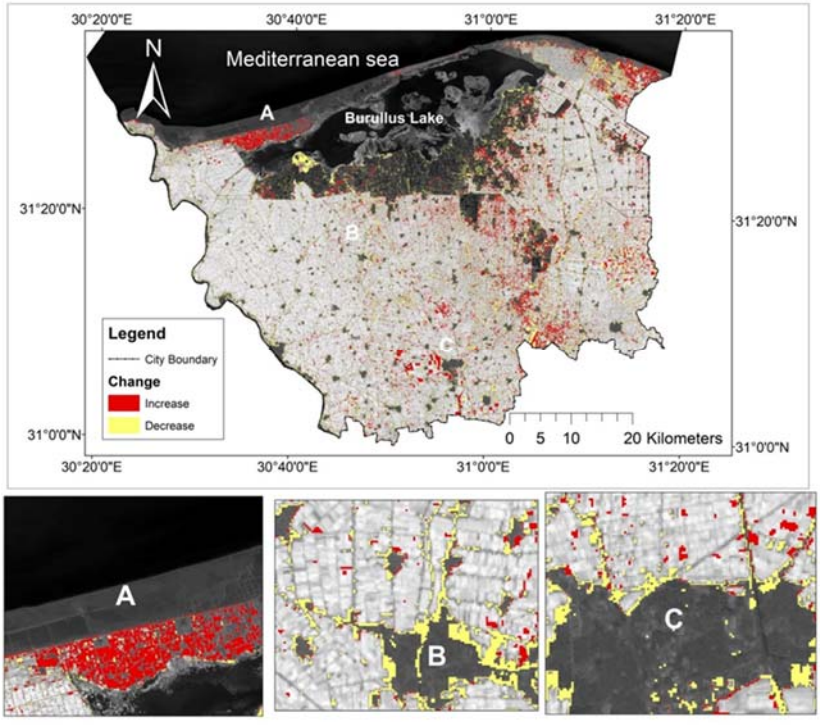

Figure 5. Changes in agricultural area between 2010 to 2016

Lake Burullus has a huge area of plants that does not include search objective because the essential goal is emphasized on cultivated areas, so the lake area has been masked from both images to increase the accuracy of results. There is interference between built-up land and soil land, thus both lands would be classified as agriculture land because both have the same purposes. Recode step has been done for merging soil lands with agriculture lands to be in the same class. The main goal from this step was to increase the accuracy of data, which reflected on the results. The last step is to detect the change between both images by using a subtraction equation, which produced an image illustrating increase and decrease areas.

The accuracy of the land cover classification has been measured by using ground truth data for the results. A stratified random sampling technique was applied for collecting the ground truth data for accuracy assessment. In this technique a minimum number of samples points was 100 for each image. The overall accuracy is determined by the sum of all samples on the diagonal divided by the total number of samples. The accuracy of both post classification images is 97% for 2016 image and 95% for 2010. The resulted accuracy of images is acceptable for the goal of study [12].

Figure 4 shows the vegetation cover of the study area (highlighted in green). In this step extraction of vegetation areas was done using NDVI index. This method is helpful for concentrating on assessing vegetation cover and removing other land cover features in the study area, which helps to increase the accuracy of the data for vegetation cover [11]. There was an overlapping between bare soli and urban land. For solving this problem, reclassifying step (recoding) was used to add soil lands to vegetation cover and that was the last step before change detection.

3. Results and Discussion

The changes in agricultural land during the period from 2010 to 2016 have been presented in Figure 5. In area (A), an increase of about 20 km² took place in the north part of Lake Burullus and other places around the lake due to agriculture reclamation. These areas are concentrated in the north part of the Lake and the eastern part of the study area. In areas (B) and (C), an excessive rate of deterioration of vegetarian cover equal about 3% of area of the study area was detected. This deterioration is concentrated around the villages and both sides of the road. The loss of agricultural land accorded not only due to urban encroachment but also due to increase of illegal fish farms. By subtracting the difference between the increase and decrease of agriculture land from the two satellite images in the period of 2010 to 2016, it was found that about 77.2 km² is the total decrease in the agriculture land of the study area. This area represents about 3.1% of total fertilized land in Kafr El-sheikh Governorate.

A previous study [13] assessed urban sprawl on agricultural soil of northern Nile Delta of Egypt by using remote sensing and GIS tools during the period between years 1984-2006. They concluded that about 689.20 km^2 of the total urban area (6.3% of total area) increased, while about 247.14 km^2 (2.26 % of total area) from agriculture land was lost during the study period. Another study [14] used GIS and remote sensing tools to monitor urban growth and land use change detection in Daqahlia Governorate during the period of 1985-2010. These results showed that about 33% of the total agricultural land was lost and about 30% of built-up area increased in the study area during the study period.

According to the results of the study, the following should be taken into consideration:

1) Urban Planning agency should cover preserve agricultural land from further urban encroachment by restricting and avoiding further expansion of the built-up area to protect agriculture sector.

2) Urban Planning agency should be concerned to develop rural areas and preserve the agriculture character. This will support agricultural area because it will increase the profit from

agriculture production for farmers, which will make farmers more concern for protecting their cultivated land.

3) GIS and remote sensing proved to be efficient tools for assessing urban encroachment. Landsat images were also efficient for studying land cover change in a big area like Kafr El-sheikh. Future studies can be conducted by using these tools with recent remote sensing images and updated data for similar studies.

4) The same methodology can be employed for investigating land cover change for other areas in Egypt, especially in the Nile Delta region.

5) The violations of illegal constructions of buildings, and fish farms that leads to urban encroachment should be abstained by enhancing the application of law in rural areas and activating strict regulations to maintain them.

4. Conclusions

Remote sensing and GIS were employed using satellite images from 2010 to 2016 to classify and analyze dramatic changes of agriculture areas. It was found that the about 3% of one the most fertilized lands of Egypt were lost between 2010 and 2016 due to urban encroachment by buildings constructions and illegal expansion of fish farms in Kafr El-sheikh. This lost not only represents a problem in food security but also has environmental and social dimensions as water pollution levels increased in Lake Burullus and limited social services are available in the expanded areas. Moreover, the new building could threaten infrastructural corrosion and its ability in absorbing the growing population which results from the new buildings that were built without planning. After the dramatic change in Egypt during 2011, the country lost a huge area of agriculture land due to several illegal violations. In order to identify the current status of these violations and find out their impacts in order to develop proper solutions further research studies are recommended by continuing studies for the whole region by remote sensing techniques using satellite imagery for monitoring urban encroachment of the study area.

5. Acknowledgements

I am grateful to my partner Dalia whom I have had the pleasure to work with during this project.

References

[1] Etim, N. E. and Dukiya, J. J. 2013. GIS Analysis of Peri-urban agricultural land encroachment in FCT, Nigeria. *International Journal of Advanced Remote Sensing and GIS*, 2(1), 303-315.

[2] Afify, H.A. 2011. Evaluation of change detection techniques for monitoring land-cover changes: a case study in new Burg El-Arab area. *Alexandria Engineering Journal* 50(2), 187-195.

[3] Kamal, A. 2004. *Monitoring, Modeling, and Managing Urban Growth in Alexandria, Egypt using Remote Sensing and GIS.* Ph.D. The Global Urban Research Unit (GURU), School of Architecture, Planning and Landscape and Geomatics Department, School of Civil Engineering and Geosciences, New Castle University, England

[4] Yikalo, H.A. and Pedro, C. 2010. Analysis and modeling of urban land cover change in Setúbal and Sesimbra, Portugal. *Remote Sensing*, 2(1), 1549-1563.

[5] Ghar, M. A., Shalaby, A. and Tateishi, R. 2004. Agricultural land monitoring in the Egyptian Nile Delta using Landsat data. *International Journal of Environmental Studies*, 1(6), 651-657.
[6] Belal, A.A. and Moghanm, F.S. 2011. Detecting urban growth using remote sensing and GIS techniques in Al Gharbiya Governorate, Egypt. *The Egyptian Journal of Remote Sensing Space Science*, 14, 73-79.
[7] Shalaby, A., 2012. Assessment of urban sprawl impact on the agricultural land in the Nile Delta of Egypt using remote sensing and digital soil map. *International Journal of Environmental Science*, 1 (4), 253-262
[8] Zaky, M. 2015. *Monitoring and Assessment of the Environmental Problems Resulting from Urban Encroachment of Western Delta Region by using Remote Sensing and Geographic Information System*. Master's thesis, Institute of Graduate Studies and Research, Alexandria University, Egypt.
[9] CAPMAS, 2017. *Egypt in Figures*: Central Agency for Public Mobilization and Statistics (CAPMAS), Cairo, April, 2017.
[10] Abdelrahman, T. 2017. Factors affecting farmers benefits from agricultural cooperatives services: the case of Kafrelsheikh Governorate, Egypt. *International Journal of Economic Research*, 14(10), 129-144.
[11] Xu, H. 2007. Extraction of urban built-up land features from Landsat imagery using a thematic oriented index combination technique. *Photogrammetric Engineering and Remote Sensing*, 73(12), 1381-1391.
[12] Almutairi, A., Warner, T.A. 2010. Change detection accuracy and image properties: a study using simulated data. *Remote Sensing*, 2, 1508-1529.
[13] Shalaby, A. and Moghanm, F.S. 2015. Assessment of urban sprawl on agricultural soil of northern Nile Delta of Egypt using RS and GIS. *Chinese Geographical Science*, 25, 274-282.
[14] Hegazy, I.R. and Kaloop, M.R. 2015. Monitoring urban growth and land use change detection with GIS and remote sensing techniques in Daqahlia Governorate Egypt. *International Journal of Sustainable Built Environment*, 4(1), 117-124.

Instructions for Authors

Current Applied Science and Technology journal contains research reports, articles concerning development work, reviews of the literature and research activities. The objectives are to publish and promote research contributions and innovative work in fields associated with applied science and technology. An electronic journal is provided on the website (https://www.tci-thaijo.org/index.php/cast/index). The Editors reserve the right to require revision of the submitted manuscript as a condition for final acceptance.

The institute and the editorial board claim no responsibility for the contents or views expressed by the authors of individual articles. Copying is allowed provided that acknowledgement is made. All articles submitted for publication will be assessed by a group of distinguished.

Ethics:

The journal is committed to maintaining the high level of integrity in the content published and has a Conflict of Interest policy in place. The journal uses plagiarism detection software to screen the submissions. If plagiarism is found, the COPE guidelines on plagiarism will be followed. For more details, please see https://www.tci-thaijo.org/index.php/cast/navigationMenu/view/Publication_Ethics.

Page Charge: Free

Submission of Manuscripts:

Manuscripts must be written in English and submitted online. Manuscripts are to be reviewed (double blinded) by at least 3 referees specializing in relevant fields. Revised manuscripts have to be sent online.

All manuscripts should be submitted to: https://www.tci-thaijo.org/index.php/cast/index

Contact:

Editor of Current Applied Science and Technology
King Mongkut's Institute of Technology Ladkrabang
1 Soi Chalongkrung 1, Ladkrabang District,
Bangkok 10520, Thailand
Tel: 662-329-8136
Fax: 662-329-8221
Email: cast@kmitl.ac.th

Manuscript Preparation Guide:

General: Manuscripts must be typewritten using *Microsoft Word for Windows,* single-spaced with margin set-up (in page set up menu) as follows (see also the document template):

Top Margin 1.5"	Bottom Margin 1.5"
Left Margin 1.5"	Right Margin 1.5"

Good quality printouts using A4 paper size are required. Format should be a single column. Times New Roman font type is required. Font sizes for various text functions are as follows:

Text functions	Size *	Typeface
Title	14 (CT)	Bold
Author and co-authors	11 (CT)	Normal
Address for correspondence	11 (CT)	Normal
Abstract and main text	10 (LJ)	Normal
Section heading and number including "Abstract", "Acknowledgement", "References"	12 (CT)	Bold
Subsection heading and number	11 (LJ)	Bold

* CT = Center Text, LJ = Left Justified.

The corresponding author should be noted (included a Fax number and E-mail address) and indicated with an asterisk. Full postal addresses must be given for all co-authors, keyed to names (if required) by superscripted Arabic numbers.

Paper Length: Should not normally exceed 10 pages including figures and tables
Spelling: American English
Abstract: Should not exceed 250 words
Keywords: Should not exceed 8 keywords
Text: Authors are requested to use the following order when typing:-

All research reports (Full Length or Short Reports): Title, Authors, Affiliations, Abstract, Keywords, Introduction (in reserch papers this must be confined to relevant matters, and must not be a general review of cognate literature), Materials and Methods, Results and Discussion, Conclusions, Acknowledgements, References.

Reviews and Discussion Papers will be considered in any format appropriate to the purposes of the authors, although adherence to the general guidelines described above is encouraged.

Line Art Figures: Figures can be drawn using several packages such as Win Draw®, Auto CAD®, Corel Draw®, VISIO® etc.

Photographs: Actual size photographs are acceptable. However, they can also be put into a text stream using a good-resolution scanner. All photographs must be clear when printed in monochrome.

Graphs: Several packages available today can produce attractive and professional graph presentation. Some also provide curve-fitting function, which can be useful. However, two-dimensional bar charts are preferred. All graphs must be clear in monochrome printing.
Equations and complex expressions: Math CAD®, Math Writer® and Equation Editor® (included in Microsoft Word®) are acceptable for presentation of this type of material.

Citations: Citations in the text should be denoted by numbers between square brackets (i.e. [1, 2], [1-3], [1, 3-8]…) *in the order of first appearance in the text.*

References: References should be numbered to correspond with the text citations. References must be arranged as follows:

Books

Authors, Initials., Year. *Title of Book.* Edition. (only include this if not the first edition) Place: Publisher.

Example:

[1] Barker, R., Kirk, J. and Munday, R.J., 1988. *Narrative Analysis*. 3rd ed. Bloomington: Indiana University Press.

Chapters of edited books

Chapter authors' surname(s), initials., Year of book. Title of chapter. In**:** Book editor(s) initials. surnames, ed. or eds. *Title of Book*. Place of publication: Publisher. Chapter number or first and last page numbers.

Example:

[2] Samson, C., 1970. Problems of information studies in history. In: S. Stone, ed. *Humanities Information Research*. Sheffield: CRUS, pp. 44-68.

E-books

Author, Year, *Title of Book*. [e-book] Place of publication: Publisher. Available through: include e-book source/database, web address or URL.

Example:

[3] Carlsen, J. and Charters, S., eds. 2007. *Global Wine Tourism*.[e-book] Wallingford: CABI Pub. Available through: Anglia Ruskin University Library website <www.libweb.anglia.ac.uk>.

Journal articles

Author, Initials., Year. Title of article. *Full Title of Journal,* Volume number (Issue number), Page numbers.

Example:

[4] Ross, A.B., Junyapoon, S., Jones, J.M., Williams, A. and Bartle, K.D., 2005. A study of different soots using pyrolysis–GC–MS and comparison with solvent extractable material. *Journal of Analytical and Applied Pyrolysis*, 74(1-2), 494-501.

Proceedings

Author, Initials., Year. Title of article. *Full Title of Proceedings*, Place of Conference, Date, page

Example:

[5] Thanaboripat, D., Ruangrattanametee, V. and Srikitkademwat, K., 2010. Control of growth and aflatoxin production of aflatoxin producing fungi in corn by salts. *Proceeding of the 8th International Symposium on Biocontrol and Biotechnology*, Pattaya, Thailand, October 4-6, 2010, 283-289.

Patent

Inventor name, Initial(s)., Assignee., Year. *Title*. Place. Patent number (status, if an application).

Example:

[6] Leonard, Y., Super Sports Limited., 2008. *Tin Can Manufacture and Method of Sealing*. Canada. Pat. 12,789, 675.

Dissertation
Author, Year of publication. *Title of Dissertation*. Level. Official name of University.
Example:
[7] Richmond, J., 2005. *Customer Expectations in the World of Electronic Banking: a Case Study of the Bank of Britain.* Ph.D. Anglia Ruskin University.

Websites
Authorship or Source, Year. *Title of document*. [online] Available at: include web site address/URL (Uniform Resource Locator).
Example:
[8] NHS Evidence, 2003. *National Library of Guidelines*. [online] Available at: http://www.library.nhs.uk/guidelines

Acknowledgements: These should be as brief as possible.

Proofs:

Proofs will be sent to the corresponding author and *must* be returned as soon as possible. Corrections should be restricted to typesetting errors.

Copyright:

The author(s) transfer(s) the copyright of the article to Current Applied Science and Technology effective if and when the article is accepted for publication.

Page Numbering:

All pages must be sequentially numbered, preferably by using the automatic page numbering function on your computer.

Copyright Material:

It is the authors' responsibility to obtain written permission from the copyright holder (usually the book or journal publisher) to use copyright material, and to send a copy of this consent with the manuscript. This consent is not normally denied but it is an international legal requirement that it be obtained.

Note:

Please note that authors are urged to check their proofs carefully before returning, since the inclusion of late corrections cannot be guaranteed.

Author(s) are responsible for ensuring that the submitted manuscript fully meets the requirements specified in the above Instructions. Manuscripts which fail to do so will be returned unedited to the Author(s) for correction in accordance with the above requirements, before they can be submitted to the processes of Referee evaluation.

1.5 ”

TEMPLATE

Enter title here (14 PT type size, Title Case, Bold, Centered)

Author Information entered here:
Name (in full)

Affiliation
City
Country
(11 pt type size, upper and lower case, centered under the title)

How to Use This Document Template

Insert the information in your document in place of the text here. For the body of your document, use Times New Roman 10 pt. Font, upper and lower case, double-spaced. Allow an extra half space above a line containing superscripts and/or below a line containing subscripts. The whole text should be left-justified. The headings should be 12 pt size, uppercase, bold and centered.

1.5” **Abstract (12pt)** 1.5”

Maximum 250 words here. (10 pt)

.....
.....
.....
.....
.....

Keywords: (10 pt)

Maximum of 8 words

*Corresponding author: Tel.: ……..... Fax: …….
E-mail: ……

1. Introduction (12 pt)

Clearly explain the nature of the problem, previous work, purpose, and contribution of the paper (10 pt).

.....
.....
.....
.....
.....

2. Materials and Methods (12 pt)

.....
.....
.....
.....

3. Results and Discussion (12 pt)

.....
.....…

4. Conclusions (12 pt)

Clearly indicate advantages, limitations and possible applications (10 pt).

.....
.....

5. Acknowledgements (12 pt)

A brief acknowledgement section may be included here (10 pt).

.....
.....

References (12 pt)

References must be numbered in the order cited in the manuscript and indicated in the text by a number in square brackets (e.g. [1, 2]) (10 pt).

Example of References must be arranged as follows:

[1] Barker, R. Kirk, J. and Munday, R.J., 1988. *Narrative Analysis*. 3rd ed. Bloomington: Indiana University Press.

[2] Samson, C., 1970. Problems of information studies in history. In: S. Stone, ed. *Humanities Information Research*. Sheffield: CRUS, pp. 44-68.

[3] Carlsen, J. and Charters, S., 2007. *Global Wine Tourism*. [e-book] Wallingford: CABI Pub. Available through: Anglia Ruskin University Library website <www.libweb.anglia.ac.uk>.

[4] Ross, A.B., Junyapoon, S., Jones, J.M., Williams, A. and Bartle, K.D., 2005. A study of different soots using pyrolysis–GC–MS and comparison with solvent extractable material. *Journal of Analytical and Applied Pyrolysis*, 74(1-2), 494-501.

[5] Thanaboripat, D., Ruangrattanametee, V. and Srikitkademwat, K., 2010. Control of growth and aflatoxin production of aflatoxin producing fungi in corn by salts. *Proceeding of the 8th International Symposium on Biocontrol and Biotechnology*, Pattaya, Thailand, October 4-6, 2010, 283-289.

[6] Leonard, Y., Super Sports Limited., 2008. *Tin Can Manufacture and Method of Sealing*. Canada. Pat. 12,789, 675.

[7] Richmond, J., 2005. *Customer Expectations in the World of Electronic Banking: a Case Study of the Bank of Britain*. Ph.D. Anglia Ruskin University.

[8] NHS Evidence, 2003. *National Library of Guidelines*. [online] Available at: http://www.library.nhs.uk/guidelines

Note:

Tables and Graphs: Minimum of 10 pt type size, all captions should be upper and lower case, centered. Each table and figure must be on a separate page (or pages if required), ***and must be embedded in the text.***

Illustrations and Photographs: Halftones, minimum of 10 pt type size, bold, captions should be in upper and lower case, centered. Images must be computer-designed with clearly visibility.

Contact

Editor of Current Applied Science and Technology
King Mongkut's Institute of Technology Ladkrabang
1 Soi Chalongkrung 1, Ladkrabang District
Bangkok 10520, Thailand
Tel: 662-329-8136 Fax: 662-329-8221
E-mail: cast@kmitl.ac.th
Website: https://www.tci-thaijo.org/index.php/cast/index

KING MONGKUT'S INSTITUTE OF TECHNOLOGY LADKRABANG

1 Soi Chalongkrung 1, Ladkrabang District Bangkok 10520, Thailand

Tel: 662-329-8136 Fax: 662-329-8221

E-mail: cast@kmitl.ac.th

Website: https://www.tci-thaijo.org/index.php/cast/index